Nanotechnology, Science and Applications

Dovepress
Taylor & Francis Group

Open Access Full Text Article

REVIEW

Two-Dimensional MXenes as Next-Generation Nanomaterials for Biosensing and Hydrogen Production

Anupam Singha Roy[1], Neelesh Babu[2], Aabid Hussain[3]

[1]School of Sciences, Woxsen University, Hyderabad, Telangana, India; [2]Department of Microbiology, School of Allied Sciences, Dev Bhoomi Uttarakhand University, Dehradun, Uttarakhand, India; [3]Department of Genomic Sciences and Systems Biology, Cleveland Clinic Research, Cleveland Clinic, Cleveland, OH, USA

Correspondence: Anupam Singha Roy; Aabid Hussain, Email singharoyanupam1@gmail.com; aabid14hussain@gmail.com; hussaia8@ccf.org

Abstract: The discovery of graphene, which has led to further research on other two-dimensional (2D) materials, has greatly enhanced the development of sustainable novel materials in the age of nanotechnology. The majority of elements in the periodic table are currently converted into 2D forms by researchers. Materials such as graphene and its derivatives, transition-metal dichalcogenides (TMDs), and transition-metal carbides (MXenes) have been extensively used because of their exceptional electronic and optical properties. While addressing synthesis challenges and stability issues, functionalization is one of the strategies used to overcome the difficulties related to the stability and large dimensions of 2D materials. This review provides detailed studies on MXene synthesis methods and their characteristic properties, emphasizing the importance of modifying MXenes for biosensing applications such as the detection of pathogenic viruses and bacteria, mycotoxins, hazardous pollutants, food contaminants, biomolecules, and cancer biomarkers. A review of the function of MXenes in hydrogen production highlights how well they improve charge transfer and lower reaction overpotentials. The future prospects of MXene-based biosensors as advanced diagnostic tools and hydrogen catalysts are also discussed, in addition to surface functionalization engineering and hybridization techniques.

Keywords: 2D materials, mxene, etching, biosensor, hydrogen production, catalyst

Introduction

Nanomaterials can be categorized, based on their dimensional structure, into zero-, one-, two-, and three-dimensional structures. Two-dimensional (2D) materials consist of one to several atomic layers, and their remarkable electrical and optical characteristics arise from the strong covalent or ionic bonds within the layers, as well as due to the weaker van der Waals forces that exist between them.[1] Graphene marked a significant advancement in science and technology as the first 2D material, due to its exceptional mechanical strength, electronic behavior, and thermal conductivity. Several other 2D materials have been discovered after the successful preparation of graphene, and this trend continues to expand. The collection of 2D layered materials has increased each year with the introduction of numerous new compounds. This extensive array of 2D materials forms a diverse family that includes a broad spectrum of properties, which can be further enhanced by combining other 2D materials with vdW heterostructures. Generally, 2D materials are classified according to their structural characteristics, including graphene and transition metal dichalcogenides (TMDs) such as WS_2, MoS_2, WSe_2, and $MoSe_2$,[2] hexagonal boron nitride (h-BN),[3] layered double hydroxides (LDHs), metal nitrides/carbides (MXenes),[4] graphitic carbon nitride (g-C_3N_4), transition metal halides (TMHs) such as PbI_2 and $MgBr_2$, transition metal oxides such as MnO_2 and MoO_3, perovskite-type oxides such as $K_2Ln_2Ti_3O_{10}$ and $RbLnTa_2O_7$[5] and 2D polymers (Figure 1). Two-dimensional (2D) materials are significant owing to their applications at the nano-and atomic scales. Ultrathin structures possess distinct electronic, magnetic, optical, and catalytic properties that distinguish them from their mass counterparts, thereby providing considerable advantages in various applications. Following exfoliation, the surfaces of these materials become exposed, leading to a significant increase in their surface area, which enhances their physical

https://doi.org/10.2147/NSA.S580785
Received: 15 December 2025
Accepted: 25 February 2026
Published: 12 March 2026

Graphical Abstract

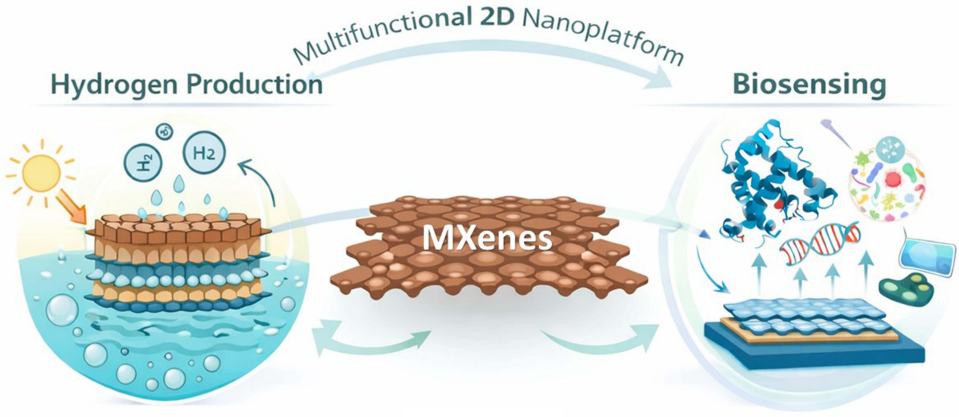

and chemical activity. Compared with their bulk counterparts, 2D semiconductor materials show significant enhancements in Coulomb interactions between charge carriers and defects, leading to the development of longer-lived excitons.

MXenes are 2D materials that are made via selective etching of the corresponding MAX phases of layered transition metal nitrides, carbides, or carbonitrides.[6] The precursor chemical formula is denoted by $M_{n+1}AX_n$, where n" changes from 1 to 4. In this formula, "M" denotes an early d-block transition metal, "A" signifies an element of groups 13 to 15 from the periodic table, and "X" denotes either nitrogen or carbon. Unlike transition-metal dichalcogenides (TMDs) and graphene, which are interconnected by van der Waals forces, MXenes are characterized by a more robust M-A bond, and the M-X bond exhibits covalent, metallic, or ionic characteristics. The chemical etching process that eliminates the A layers depends on the metallic nature of the M-A bond, leading to the formation of MXenes.[7] MXene is synthesized via a selective etching process that utilizes the chemical formula $M_{n+1}X_nT_x$, where T signifies the termination functional groups (such as–F,–OH,–Cl, or–O) and x indicates the quantity of these groups. The presence of these surface termination groups and the chemical etching method creates a hydrophilic nature on the MXene surface. Furthermore, these terminal functional groups play a key role in influencing the ion transport and electrical characteristics of MXene. In 2011, Barsoum and Gogotsi identified $Ti_3C_2T_x$. They employed hydrofluoric (HF) acid to extract $Ti_3C_2T_x$ from its precursor MAX phase, Ti_3AlC.[8] To date, over 100 MAX phases have been produced through various combinations of the three constituent components of MAX phases.[9] Although MXenes show promising characteristics, only about 30 variants have been synthesized and their properties evaluated experimentally. This provides a significant opportunity for the identification of new MXenes with unique properties. MXenes are significant in numerous technological applications owing to their diverse chemical characteristics and extensive potential for surface functionalization. Their roles include energy storage, catalysis, sensing, lubrication, and electromagnetic interference shielding. As an electrode, MXene offers distinct benefits for electrochemical energy storage systems, gathering keen interest as it emerges as a leading-edge

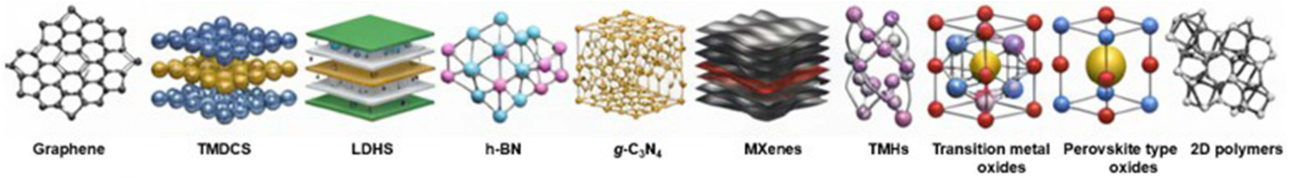

Figure 1 Various 2D materials.
Abbreviations: TMDCS, Transition Metal Dichalcogenides; LDHS, Layered double hydroxides; h-BN, Hexagonal boron nitride; g-C_3N_4, Graphitic carbon nitride; TMHs, Transition metal halides.

https://doi.org/10.2147/NSA.S580785

electrode material for supercapacitors.[10] The challenges related to the agglomeration and accumulation of MXene materials, along with the impact of their surface functional groups on capacitor performance, significantly hinder the real-world uses of MXenes. To enhance the energy storage capabilities, researchers have explored the combination of MXenes with several materials, such as metal oxides or hydroxides, polymers, and carbon-based substances, taking advantage of the benefits offered by these composite materials. Consequently, a variety of MXene composites with remarkable energy storage performances have been developed.

Figure 2 illustrates the growing research interest in MXenes and their applications in biosensing and hydrogen production based on Scopus-indexed publications from 2017 to 2025 (24 November). Analyses were performed on Scopus during the literature review using the keyword "MXene". Specifically, searching for this term in the titles, abstracts, and keywords resulted in 19,829 records as of November 24, 2025. The keyword search indicated a significant increase in the number of MXene-related publications from 2017 to the present (Figure 2a). Figure 2b shows the number of publications related to their application in biosensing and hydrogen production. The exponential increase in publications indicates the advancement of MXenes and their critical role in biosensing and hydrogen production.

Currently, the progress of MXene-based biosensors has become a favourable field, especially for applications in health and environmental monitoring.[11] MXenes exhibit numerous beneficial properties, including large surface area, high electrical conductivity, exceptional hydrophilicity, and ease of surface modification, making them ideal candidates for the development of biosensors.[12] Additionally, their relevance for biosensing applications is further enhanced by their stability in aqueous environments and biocompatibility.[13] Among the various MXenes, Ti_3C_2 MXene stands out due to its large surface area, exceptional conductivity, significant hydrophilicity, and remarkable absorption capacity, making it ideal for biosensor applications.[14] MXene-based biosensors have shown great potential in the medical field for detecting different biomarkers, pathogens, and metabolites.[15] Recently highly sensitive and selective sensors have been developed for checking glucose levels,[16] discovering cancer biomarkers,[17,18] and finding infectious agents.[19,20] Tian et al synthesized ferrocene (Fc)-modified HDNA2 N-carboxymethyl chitosan/Mo_2C biosensor to detect hairpin DNA1 and hairpin DNA2 in the presence of miRNA-21.[21] In addition to having a high affinity to the DNA probe, the linear range of the chitosan/Mo_2C nanocomposite varies from 1.0 nm to 1.0 nM, with a LOD of 0.34 fM Rapid diagnostics and continuous health monitoring are made possible by these sensors, which have the potential to renovate personalized medicine and enable early detection of disease.

The antibacterial properties of MXene have been reported.[22] The antibacterial effects of $Ti_3C_2T_x$ MXene suspensions were studied by Rasool et al.[23] Their research revealed that both single-and layered $Ti_3C_2T_x$ flakes in a colloidal solution exhibited enhanced antimicrobial properties against *B subtilis* and *E coli* compared to graphene oxide (GO), a well-established antimicrobial substance. Recently, the COVID-19 detecting capabilities of MXenes have been

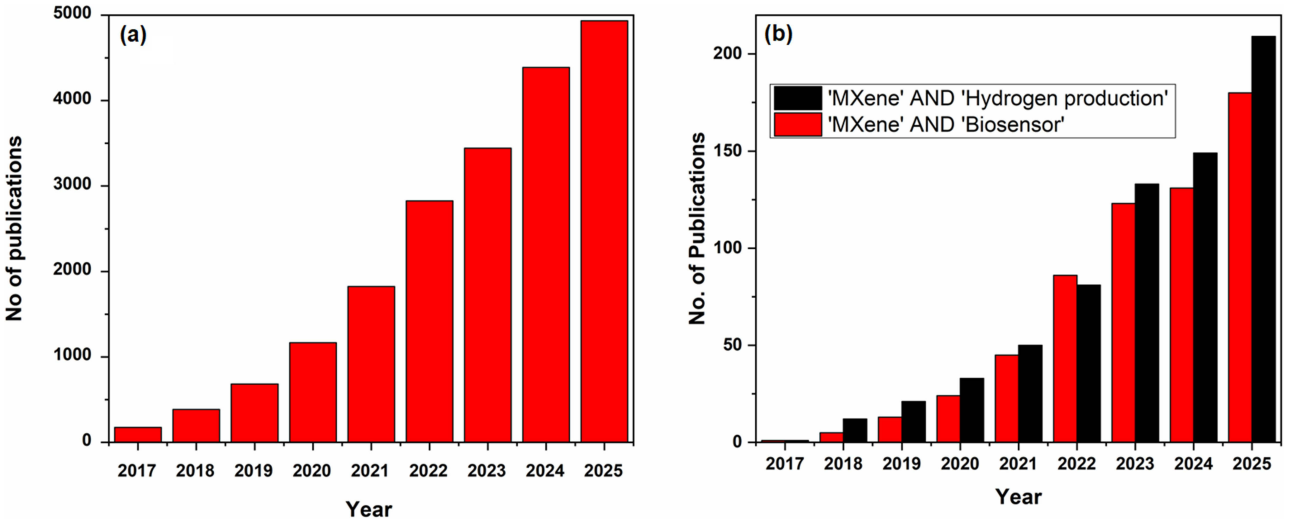

Figure 2 (**a**) Trend of research publications on MXenes, (**b**) Trend of research publications on biosensor and hydrogen production using MXenes.

https://doi.org/10.2147/NSA.S580785

examined and published.[24] Additionally, Li et al examined the sensing abilities of MXene against different concentrations of antigens from both 2019-nCoV and the influenza virus using a cost-effective MXene-graphene field-effect transistor (FET) sensor integrated with a microfluidic channel, which captures viruses in solution.[25] Recently, research has been conducted on the preparation of amino-silane-functionalized Ti_3C_2 nanosheets using a slightly rigorous layer delamination method.[26] The MXene functionalized with amino groups provided a dependable substance for the covalent immobilization of cancer bio-receptors aimed at identifying cancer biomarkers, such as carcinoembryonic antigen. Notable improvements have also been made in the environmental applications of MXene-based biosensors. Scientists have engineered sensors with high sensitivity and specificity to detect pollutants,[27] heavy metals,[28] and hazardous chemicals in water and air.[29] These can improve water and air monitoring, control pollution, and address global challenges related to water and air pollution. The combined use of MXenes and other nanomaterials as well as advanced sensing technologies has led to significant advancements. For example, MXenes combined with aptamers, antibodies, or enzymes have created highly specific and sensitive biosensors.[30] Moreover, MXenes have been integrated into electrochemical, optical, and field-effect transistor-based sensors and have shown enhanced detection limits and quicker response times.[31]

Hydrogen has emerged as a remarkable alternative fuel for the future because of its energy density of 120 MJ/kg, which is far above that of gasoline. Hydrogen has gained significant interest as a sustainable alternative energy source and a green energy carrier. However, compared with other production techniques, electrochemical water splitting has several advantages: fast reaction kinetics, production of high-purity hydrogen, and absence of greenhouse gases. The use of novel materials to improve the efficiency of hydrogen production has increased significantly in recent years. The hydrogen evolution reaction (HER), which greatly increases the efficiency of hydrogen evolution, is made possible by the exceptional electrocatalytic qualities.[32] MXenes are especially suitable for use in electrochemical water splitting owing to their exceptional structural and electronic properties.[33] Studies on MXenes have demonstrated their efficiency in various methods of hydrogen production, especially in electrocatalytic reactions, where they have been shown to enhance the hydrogen production rate. Many metals in MXenes exhibit favorable hydrogen adsorption from a catalytic standpoint, encouraging the effective kinetics of hydrogen production. Consequently, the use of these metals in the synthesis of catalysts from MXenes has increased. According to recent studies, MXenes have exceptional catalytic support qualities, and the addition of transition metals such as Ru significantly improves their electrocatalytic performance.[34] Furthermore, their efficiency as electrocatalysts is greatly increased by their natural capability to absorb hydrogen and enable proton transfer. These qualities increase the potential of MXenes as cutting-edge materials for sustainable energy solutions by making them ideal for incorporation into renewable energy systems and large-scale hydrogen production.

This review begins by presenting an overview of the characteristics of MXene materials, along with various preparation techniques such as etching with HF and fluorine salts, electrochemical etching, base etching, Lewis acid molten salt etching, and direct synthesis. This review also discusses in detail their applications in photocatalytic hydrogen generation and water electrolysis, highlighting recent developments and challenges in sustainable hydrogen production using MXenes. In previous years, many researchers have thoroughly explored the synthesis, characterization, and applications of MXene materials in their articles. Sinha et al discussed an outline of the applications of electrochemical, gas-absorptive, and piezoresistive sensors.[35] The use of MXene materials as biosensor was discussed by Ozcan et al,[36] whereas Yoon et al focused on MXene nanocomposite-based electrochemical biosensors.[19] However, there is a scarcity of reviews that specifically concentrate on both biosensing applications and hydrogen production using MXene materials. Furthermore, advancements in the research on the use of MXene in sensors and environmental pollution removal are highlighted. The challenges and potential opportunities associated with MXenes in other fields are discussed at the end of this review.

Synthesis Methods for 2D Materials

The top-down and bottom-up methods are commonly used to produce 2D materials (Figure 3). To separate the layers and create 2D materials, top-down techniques exfoliate the bulk materials using physical or chemical processes. This

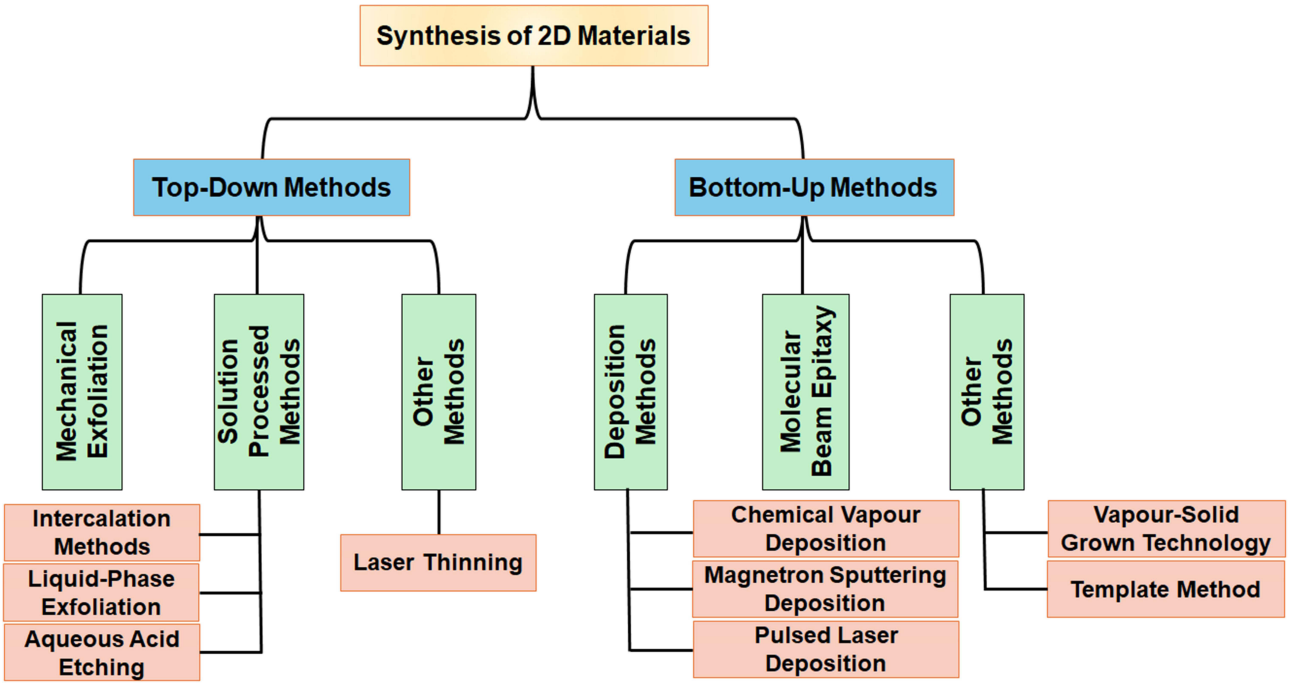

Figure 3 Various synthesis methods of 2D materials.

effectively overcomes the van der Waals forces that hold layers together. Bottom-up approaches concentrate on the direct growth or deposition of two-dimensional materials onto a substrate.

Bottom-Up Approaches

Chemical Vapor Deposition (CVD) is the primary method employed for bottom-up synthesis of 2D materials. This technique has been utilized to create 2D layers of graphene,[37] h-BN,[38] and MoS_2.[39] One of the key benefits of CVD over mechanical or chemical exfoliation is its ability to produce large-area films, making the process more efficient. For instance, CVD has enabled the roll-to-roll production of films composed of graphene, which is suitable for applications as transparent electrodes. This method is particularly significant when there is no equivalent 3D layered form for 2D materials. Silicene illustrates this fact, as it lacks any 3D layered form; thus, the controlled accumulation of silicon on a substrate such as silver.[40]

Top-Down Approaches

Mechanical Exfoliation

Most layered materials have relatively weak interlayer bonds, such as hydrogen or van der Waals interactions, which facilitate layer separation. These materials facilitate the mechanical exfoliation of 2D layers from 3D crystals by cutting one layer from another. Novoselov was the first to use Scotch tape to peel off graphene layers to separate individual layers from highly oriented pyrolytic graphite.[41] The electronic properties of the individual graphene layers could be investigated using this technique. The rubbing of 3D materials against paper is another mechanical method similar to writing chalk on a blackboard or using a graphite pencil on paper. Mechanical exfoliation has been applied to various layered materials beyond graphene, such as h-BN, TMDs, MoO_3, and hydrated WO_3.[42]

Chemical Exfoliation

Chemical exfoliation can be used to construct a wide range of 2D materials from 3D layered structures such as graphene, graphene oxide, h-BN, TMDs, metal oxides or hydroxides, and clay. The basic idea of using chemical exfoliation involves disturbing the interactions between the layers using different techniques that can be purely chemical, chemical-

https://doi.org/10.2147/NSA.S580785

thermal, and chemical-mechanical. Most of these techniques are performed in a liquid medium. An example of this interaction is the reaction between graphite and a mixture of HNO_3 and H_2SO_4, in combination with potassium chlorate, resulting in the oxidation of graphite. Subsequently, thermal shock heating the material to 1050°C for 30 seconds decomposes the intercalant, resulting in a significant volume increase that separates the 2D graphene oxide layers.[43] Sonication-aided exfoliation can be employed as an alternative of thermal shock to achieve the same effect on the intercalated GO layers.[44] TMDs can also be exfoliated by sonication in various solvents, such as N-methyl-pyrrolidone or isopropanol. Similarly, graphene sheets can be exfoliated by sonication in water along with a surfactant. Modification of the interlayer composition by a chemical process is required when the bonds between the layers are too strong to break. Heating SiC single crystals under high-vacuum or argon conditions sublimates silicon and creates graphene.

Preparation of 2D MXenes

MXenes are usually prepared by selective etching of atomic layers from the MAX phase, which can consist of various elements such as Al, Si, Ga, and/or Sn, using various techniques. This is possible when the metallic bond M-A in the MAX phase is weaker than the covalent bond M-X, which makes it reasonable to etch A atoms selectively without affecting the covalent M–X bonds. In recent years, much attention has been focused on developing various techniques for MXene preparation, especially economical and energy-efficient techniques. The concepts of clean production and green chemistry should also be considered during the preparation of the MAX phase. To date, MXene has usually been prepared from the MAX phase using various techniques, such as fluoride etching, electrochemical etching, molten salt etching, and direct preparation techniques (Figure 4), which are further explained in this section. Table 1 presents a comparative analysis of various techniques used to synthesize MXenes.

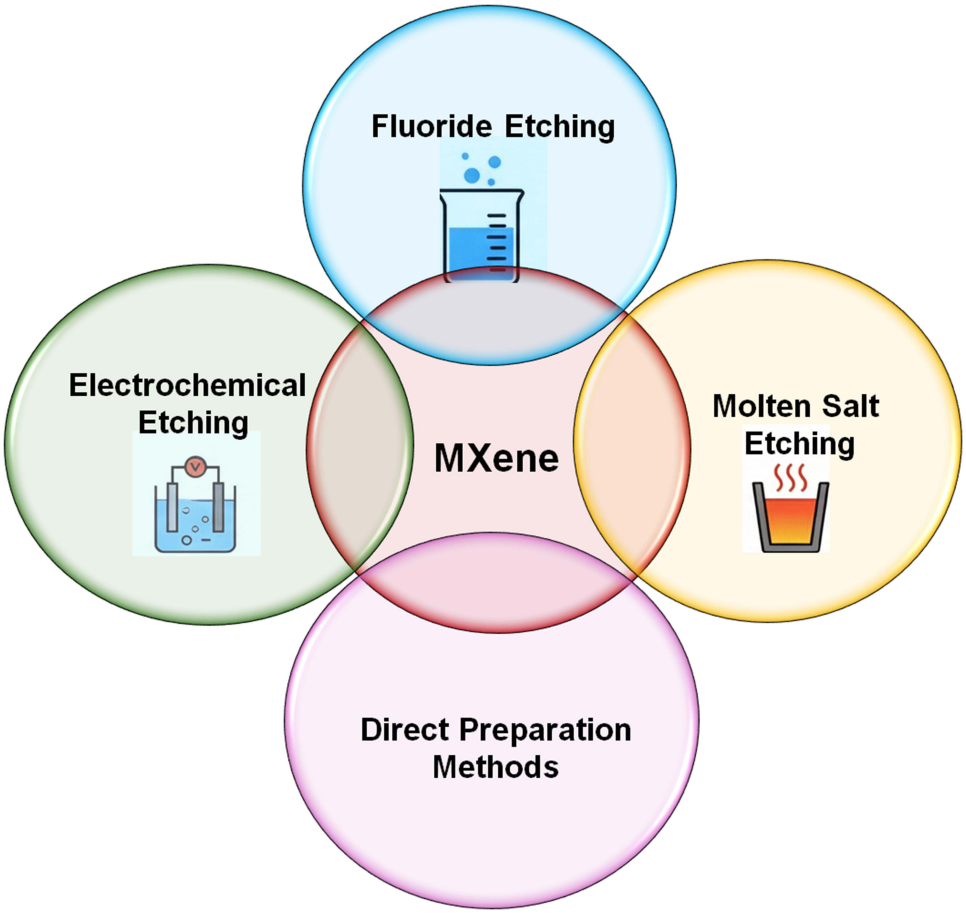

Figure 4 Different synthesis methods of MXenes.

Table 1 Different Etching Methods for the Synthesis of MXenes

Methods	Advantages	Disadvantages
Fluoride etching	• Can be performed at room temperature • Small flake size • Surface functionalization by -F, -OH, and -O in one step	• Extremely corrosive and toxic • Require safety measures • Damage in layered structure • Restriction in large scale production
Electrochemical Etching	• Avoid use of HF • MAX phase can be reused • Chemically resist MAX phase can be used • Use of gentle electrolyte	• Low yield of product • Depend on electrode surface area • Over etching produce carbon impurity
Lewis Acid Molten Salt Methods	• Green and viable route • No liquid acids require • Surface with -Cl or – Br termination	• Inert atmosphere • Special equipment • High temperature • Mixed salt impurities

Etching Using HF and/or Fluoride Salts

When HF was used as an etchant, the chemical bonds between elements A and M were sufficiently strong to destroy the parent phase material. Mashtalir et al reported the dynamic control of selective aluminum corrosion from Ti_3AlC_2 in a 50% HF solution.[45] The results showed that the progress of the fast phase transformation from the bulk Ti_3AlC_2 to the $Ti_3C_2T_x$ is favored by increasing the temperature of sinking, extending the time for reaction, and decreasing the size of the initial particles. They further confirmed that single-layered $Ti_3C_2T_x$ MXene can be exfoliated during HF etching. Wang et al also prepared $Ti_3C_2T_x$ MXene from the Ti_3AlC_2 powder using 50% HF at room temperature.[46] In such a process, -OH or -F groups formed on the surface and edges of the MXene with accordion-like morphology. In addition, HF is an excellent etchant that allows the generation of $Ti_3C_2T_x$ flakes with relatively small lateral dimensions. Although HF etching is a simple and widely applicable method for the preparation of MXenes, the toxicity and safety risks of this process are high, and the resultant MXene may suffer from various types of defects.

Studies have shown that HF synthesized in situ using a mixture of salts such as LiF, NaF, CaF_2, and HCl or H_2SO_4 possesses etching properties similar to those of pristine HF. This in situ-synthesized HF yielded MXene flakes with a longer size and fewer nanodefects compared to flakes obtained from conventional HF etching. For example, Ghidiu et al obtained $Ti_3C_2T_x$ MXene using LiF and HCl solution-based etching, yielding a lattice constant of around 27–28 nm, compared to 20 nm for $Ti_3C_2T_x$ using pristine HF.[47] This increase in lattice constant due to corrosion using a LiF+HCl solution has been attributed to an increase in interlayer distance, thereby increasing the electrochemically available surface area and promoting ion diffusion in electrolytes. LiF- and HCl-etched MXenes usually have functional groups of –F, –OH, and –O, but usually have fewer –F terminals than those derived from direct HF. This resulted in improved electrical and catalytic properties. However, studies have shown that Ti_3C_2 flakes derived using a precursor with in situ fluoride salt/HCl etching exhibited better performance in the HER than those derived using direct HF, possibly owing to fewer –F terminations and a favorable layer composition.[48] Other mild etching agents such as NH_4HF_2 can also provide in situ HF on precursor surfaces without side reactions that are harmful to human health. Li^+ and NH_4^+ are also used as intercalation agents to produce $Ti_3C_2T_x$ MXene flakes that are free of Al sublayers with an increased interlayer distance. Adibah et al also investigated how in situ HF and direct HF affect Ti_2C_3 MXene morphology using a precursor of Ti_2AlC_3.[49]

Fluoride-Free (Electrochemical) Etching

Electrochemical etching is a highly effective technique for the fabrication of high-performance 2D $Ti_3C_2T_x$ MXenes. This process can be conducted in fluoride-free electrolytes, resulting in $Ti_3C_2T_x$ that does not contain fluorine terminations. Unlike other chemical etching techniques that use HF or LiF/HCl, the electrochemical etching technique does not use any F ions. The developing MXenes contained only Cl, O, and OH groups. By maintaining a steady voltage, careful etching of the aluminum layers could be accomplished using Cl−ions. A novel electrochemical process was introduced by Feng et al, which employs double aqueous electrolytes for the packing of Ti_3C_2.[50] Li et al successfully synthesized

highly pure multilayer MXene through alkali-assisted hydrothermal methods derived from the Bayer process.[51] The surface modification of MXene was achieved by oxidizing a Ti_3AlC_2 solution with NaOH, followed by dissolution in $Al(OH)_4$. This process leads to the further oxidation of the inner Al atoms, resulting in the formation of new dehydrated oxide hydroxides (AlO(OH) and simple $Al(OH)_3$. The Ti layers serve as lattice confinement, inhibiting insoluble compounds from easily reacting with -OH to form soluble $Al(OH)_4$, which could hinder MXene synthesis. Selective etching of the MAX phase using strong alkali can produce hydrophilic products with fluorine-free termination. Transition metal halides serve as electron acceptors and potentially interact with the A layer of the MAX phase in the molten form. Li et al proposed an innovative technique for etching MAX phases via a direct redox coupling reaction of elemental A and a cation from a Lewis acid molten salt.[52] Nevertheless, excessive etching of the MAX phase into carbine-derived carbon (CDC) is a problem associated with electrochemical etching. A core-shell representation was suggested to explain the process by which Ti_2AlC was electrochemically etched into Ti_2CT_x and CDC. This model highlights the necessity of carefully balancing the etching parameters to produce MXenes, while preventing overloading. Scientists have made significant efforts to achieve these goals. They successfully developed MXene products with excellent electrochemical properties by utilizing organic materials and deep eutectic solvents (DES) as etching solvents. Ti_3C_2 MXene can be produced in DES through a highly dependable and anhydrous ion thermal process.[53]

Thermal-aided electrochemical etching was used for the synthesis of Ti_2CT_x, Cr_2CT_x, and V_2CT_x.[54] The use of dil HCl, as an etchant, combined with mild heating accelerated the etching of the MAX phase. The synthesis of Ti_2CT_x via electrochemical etching occurred via a two-step approach. During 1st stage, Al atoms were initially extracted from the layered structure owing to the applied voltage because it was easier to break the Ti-Al bond than the Ti-C bond. In the 2nd stage, both Al and Ti species were entirely removed, resulting in only monolayer carbon atoms. MXenes with various structures can be produced by adjusting temperature, etching time, and electrodes. This process also successfully yields two additional MXenes (V_2C and Cr_2C), which are typically regarded as challenging to synthesize. Previous studies have indicated that V_2C requires HF etching for over two days, with HF concentrations reaching as high as 50%. Thermally assisted electrochemical etching not only introduces a complete method for synthesizing MXenes but also enables the fabrication of those that are difficult to produce. This approach can be used for rapid, easy, and safe preparation of MXenes.

Lewis Acid-Molten Salt Etching Method

In addition to the above-mentioned etching procedures, there are other methods for extracting A-layer atoms from MAX phases using molten salts. After the synthesis of MXenes via molten Lewis acids, Huang et al engaged in comprehensive and systematic research on proposing a method for making MXenes using a general molten salt.[55] The redox potential of the Lewis acid cations was high enough to oxidize the A-layer atoms in the MAX phase. Several molten salts ($CdCl_2$, $CoCl_2$, $CuCl_2$, $FeCl_2$, $NiCl_2$, AgCl) were utilized to etch various MAX phases (Ti_2AlC, Ti_3AlC_2, Ti_3AlCN, Nb_2AlC, Ta_2AlC, Ti_2ZnC, Ti_3ZnC_2) to produce the subsequent MXenes. These findings indicate that, in the conventional MAX phase, metal A can be replaced with late-transition metal halides. This finding significantly broadened the scope of MAX phases as MXene precursors. A method that does not involve HF, and thus Lewis acid etching, is an environmentally friendly approach for the preparation of MXene. Li et al successfully synthesized a Ti_3ZnC_2 MAX phase from Ti_3AlC_2 and Lewis acidic molten salt $ZnCl_2$ via a displacement reaction at a temperature of 550°C. By increasing the ratio of MAX:$ZnCl_2$, Ti_3ZnC_2 can be further converted into $Ti_3C_2Cl_2$ MXene.[56] Talapin group produced several MXenes with -Cl surface modifications in $CdCl_2$ molten salt and produced a series of MXenes with bromine (-Br) surface terminations using Lewis acidic $CdBr_2$, thus broadening the molten salt etching method from chlorides to other halides.[57] Sajid et al enhanced the method by utilizing a $ZnCl_2$ molten salt, which led to the production of $Ti_3C_2Cl_2$ MXenes without any residual fluorine.[58] This resulted in a clean surface and modified electronic features, ultimately improving the HER activity of these chloride terminated MXenes.

Direct Preparation Method

Researchers have also investigated the application of CVD as a method for preparing MXenes, in contrast to the previously mentioned approach for selective removal of A-layer atoms from the MAX phase via chemical etching.

Dmitri V Talapin et al established a CVD technique in which titanium chloride ($TiCl_3$ or $TiCl_4$), and an additional source of carbon or nitrogen (such as graphite, CH_4, or N_2) as precursors for MXenes synthesis, including the commonly utilized Ti_2CCl_2.[59] This innovative direct synthesis technique not only reduces time and eliminates the hazardous waste associated with the etching process but also enhances the efficiency of MXene production, thereby facilitating the advancement of industrial applications for these materials. The hydrothermal method is effective for large-scale production of MXenes featuring diverse designs, as it eliminates the need for exposure to highly hazardous HF. Al layers were created through the MAX phase using an innovative leaching technique that eliminates the use of fluorine hydrothermal treatment. The process involves immersing Ti_3AlC_2 in an aqueous NaOH solution for 100 h, followed by a 15 h hydrothermal process with 1 mol/L H_2SO_4 at 85°C.[60] Another technique for synthesizing $Ti_3C_2T_x$ includes immersing small Ti_3AlC_2 particles in water containing NH_4F before undergoing the hydrothermal reaction.

Properties of MXenes

MXene possesses abundant oxidation-reduction sites, resulting in improved capacity levels. In the case of $Ti_3C_2T_x$ MXene, the oxidation state of titanium varies continuously owing to the hydration of the oxygen-containing functional groups, which enhances the charge transfer ability of the transition metal in its valence state.[61] The =O functional groups exhibit greater stability compared to the-OH and -F groups because of their ability to share a higher number of electrons with M within the MXene layer. This electron sharing facilitates the interconversion between the =O and -OH end groups during charge/discharge cycles, resulting in an abundance of active sites for redox reactions.[62] The individual layered assembly of 2D MXene contributes to an increased surface area, which enhances ion intercalation and transport.[63] Furthermore, the layered configuration of MXene enables compatibility with various intercalating agents, thereby broadening its electrochemical activity. This improves the pseudocapacitance and cycling stability. The notable energy-storage capabilities of MXene are evident in various devices constructed based on it, showing high energy and power densities.

MXenes exhibit extraordinary conductivity, and their composition includes various transition metals such as Ti and Mo, which are known for their high conductivity. These metals create conductive pathways within the MXene structure, facilitating electron flow and enhancing the overall conductivity of the material.[64] MXene allows for greater electron availability because they are two-dimensional (2D) material with a large specific surface area. This enables electrons to move freely across the 2D plane, minimizing electron losses and thereby enhancing conductivity. The structure of MXene significantly influences its conductivity; single-layer and larger flakes exhibit superior interactions compared with multilayered and smaller flakes. Furthermore, in contrast to other 2D materials like metal sulfides, hydroxides or graphene, MXene possesses a variety of functional groups, including -OH and -F. Modification of the functional groups would represent a means to tune its electronic structures and charge transfer properties, thus impacting its conductivity performance.[65] The combination of transition metals and functional groups makes MXene an outstanding conductive material with numerous potential applications. The remarkable conductivity of MXene enables rapid electron flow, which in turn enables the development of high-energy-density supercapacitors.

MXene exhibits significant hydrophilicity because of the abundant–OH and -F functional groups present in its layered structures.[66] This composition results in a highly polar MXene surface. When in contact with water, these polar functional groups are capable of forming hydrogen bonds with H_2O, enhancing the attractive forces between MXene and H_2O.[67] The hydrophilicity of MXene can be enhanced owing to its inherent features, including a high specific surface area and porous structure. This characteristic provides MXene with remarkable dispersion, stability, and potential for application in water.

MXene is composed of multiple layers of 2D nanosheets stacked via relaxed bonding. Additionally, by intercalating various materials such as polymers or liquids, the layered structure of MXene can be significantly enhanced, leading to the formation of composite materials and improved flexibility. The mechanical characteristics of MXenes are affected by various factors, including their structural composition, dimensions, defects, incomplete edges of nanosheets, and surface terminal groups. The surface terminal groups play an important role in enhancing the mechanical properties of MXenes. For instance, the presence of =O terminal groups strongly enhances the interlayer interactions, which improves the shear and strain resistance performance. By utilizing the contact surface area, the interaction with the external environment can

be maximized, leading to reduced stress concentration. This enhancement allows for greater displacement and deformation capacity which improves the flexibility and durability of MXenes and mitigates the effects of outside vibrations on the inner structure of capacitors.[68] Furthermore, research conducted by Guo et al indicates that the introduction of =O terminal groups under both uniaxial and biaxial conditions resulted in an increase in the tensile range of Ti_2C to 28% and 20%, respectively. This finding suggests that surface terminal groups effectively inhibit the collapse of Ti_2C.[69]

Applications of MXenes

Applications of 2D MXenes as Biosensors

Owing to their special qualities, MXenes have received considerable interest for biosensing applications (Figure 5). MXenes can interact with biomolecules via hydrogen bonding, van der Waals interactions, electrostatic interactions, or ligand binding owing to their hydrophilic surface groups (–OH, =O, and–F). MXenes are exceptional candidates for use as carriers in biosensor device applications because of this feature.[70] Different MXene compositions have shown non-cytotoxicity and biocompatibility, further confirming their potential for biomedical applications.

Sensor for Biomolecules

Small biomolecules, such as glucose, ascorbic acid, cholesterol, and neurotransmitters, such as dopamine, glutamate, and uric acid, are important for daily human activities and the body's resistance to illness. Therefore, in order to effectively monitor human health, it is essential to quickly and easily identify these biomolecules.[71] Conventional methods of biomolecule monitoring include colorimetry, spectrometry, and HPLC. However, these techniques have certain

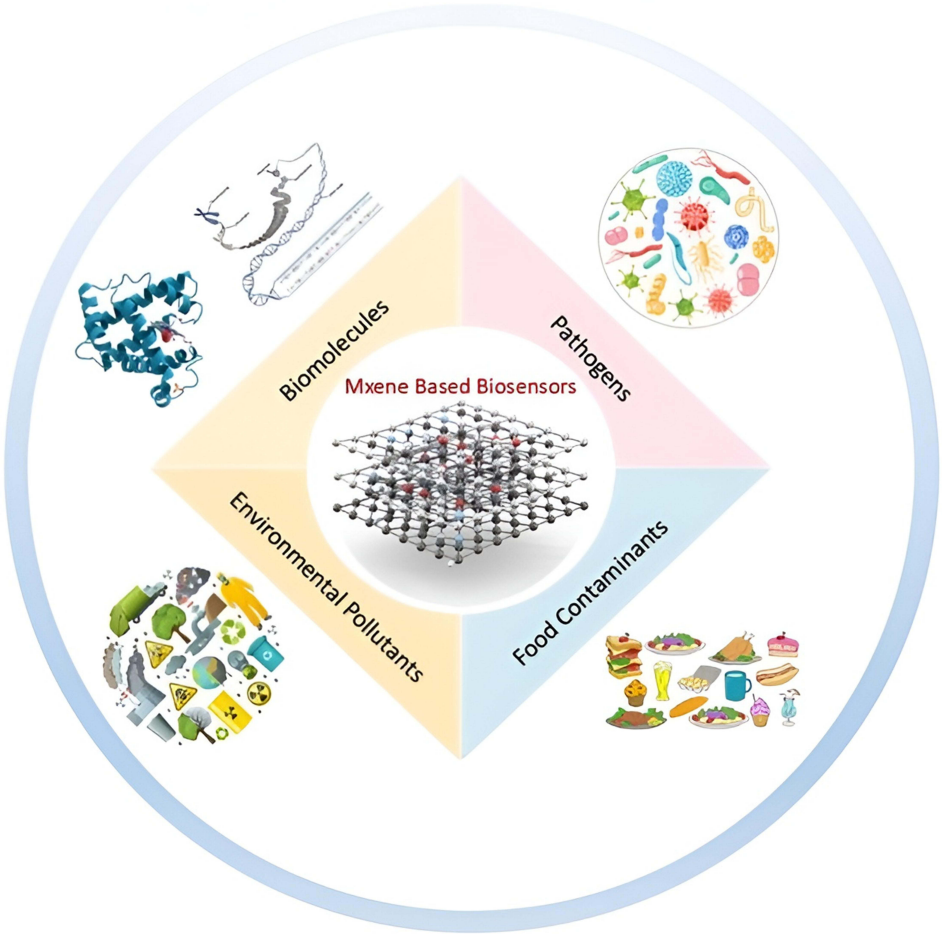

Figure 5 Applications of MXenes as Biosensors.

drawbacks, including lengthy processing times, expensive reagents, complicated extraction procedures, and high training requirements. Biosensors have recently become popular for the detection of biomolecules because of their high sensitivity, selectivity, compatibility, stability, and low cost. Biosensors are fabricated using a variety of metal nanoparticles, metal oxides, metal carbides/nitride nanoparticles, or nanosheets to enhance their performance. Among these nanomaterials, MXene provides a large number of efficient surface sites that are suitable for immobilizing bioreceptors and improving the selectivity, stability, sensitivity, and accuracy of biosensors.

Ti_3C_2 was synthesized by Xu et al using the hydrothermal method to identify intracellular glutathione (GSH), a vital biomarker for both health and illness.[72] Due to surface flaws and quantum confinement effects, the Ti_3C_2 displayed a blue emission. In the presence of GSH, Förster resonance energy transfer (FRET) occurs from Ti_3C_2 to GSH over a broad concentration range (1–100 μM), making it possible to detect GSH concentrations as low as 0.02 μM GSH-functionalized Ti_3C_2 has also been reported to be a significant biomarker for uric acid.[73] In which the uricase enzyme first oxidizes uric acid into allantoin and H_2O_2, and the horseradish peroxidase enzyme oxidizes *o*-phenylenediamine (OPD) to yellow-colored 2,3-diaminophenazine (oxOPD). The oxOPD product was emitted at 568 nm, and GSH@Ti_3C_2 was efficiently emitted at 425 nm. The addition of uric acid to the composite of GSH@Ti_3C_2 and oxOPD leads to FRET, which causes the 568 nm emission to increase and GSH@Ti_3C_2 425 nm emission to decrease. This sensing nanoplatform allowed uric acid to be detected within a concentration range of 1.2–75 μM with a detection limit of 125 nM.

Red-emitting carbon dots (RCDs) and Ti_3C_2 MXene nanosheets were used by Zhu et al to develop a glucose sensor.[74] Ti_3C_2 nanosheets successfully reduced the fluorescence intensity of RCDs by more than 96% (Figure 6a and b), which is then restored upon interaction with glucose. To prevent IFE from RCDs to Ti_3C_2 MXene nanosheets, glucose oxidase aids in the oxidation of glucose, which produces H_2O_2 and oxidizes Ti_3C_2 to Ti $(OH)_4$. To investigate simple, sensitive, and effective methods for cholesterol measurement, a $Ti_3C_2T_x$ MXene-based enzymatic biosensor for cholesterol measurement was developed by Xia et al.[75] Using chitosan and MXene as supporting materials, they immobilized the cholesterol oxidase (ChO_x) enzyme onto the electrode surface to construct a biosensor (Figure 6c). Shahzad et al introduced an electrochemical biosensor based on MXene technology for detecting dopamine (DA).[76] This biosensor provides a broad detection range for DA (0.015–10 mM) and has a limit of detection (LOD) of 3 nM. Table 2 summarizes MXene-based biosensors designed to detect biomolecules.

Sensor for Pathogens

Pandemics are primarily caused by pathogenic bacteria and viruses. The initial detection of these viruses and pathogenic bacteria is crucial for accurate diagnosis and minimizing disease fatality, as well as for effective control of the spread of these pathogens. Owing to its exceptional electrical conductivity and optical properties, MXene is an ideal option for the application of biosensors in pathogenic bacteria and viruses.[84] MXene offers a large number of effective sites for immobilizing bioreceptors on the surface, which improves the sensitivity, selectivity, and accuracy of the biosensor.

The global healthcare system faces several challenges owing to the serious health impact of severe acute respiratory syndrome coronavirus 2 (SARS-CoV-2) infection. An effective biosensing technique was developed by a research team to detect viruses using an amino-functionalized probe DNA. The immobilization of NH_2-pDNA on the $Ti_3C_2T_x$ MXene nanosheet-modified SPCE has been shown successfully by Bharti et al.[79] The novel technique developed by the researchers enabled the result within 12 min with a high level of sensitivity in the following range (0.1 pM to 1 μM), with a detection limit of 0.004 pM. The results obtained in the spiked serum samples displayed equal sensitivity, with a detection limit of 0.003 pM and a linear range of 1 pM to 1 μM. This result is significant because it was obtained in a real-world trial setup, indicating its high potential for real-world applications.

To create an MXene-based biosensor for virus detection, Chen et al developed a DNA-functionalized chemoresistive biosensor designed for the selective and efficient detection of the nucleocapsid gene of SARS-CoV-2.[80] This study involved the construction of a biosensor by noncovalently loading a probe DNA molecule onto 2D $Ti_3C_2T_x$ MXene. After the SARS-CoV-2-N gene hybridized with the ssDNA probe on the MXene surface, the conductance of the sensing channel increased; however, no signal was observed for non-complementary targets (SARS-CoV-1 N and MERS-CoV N genes), indicating the high specificity of the biosensor. Figure 7 shows how the DNA-functionalized MXene sensor can detect the SARS-CoV-2 N gene in saliva with a limit of detection (LOD) of less than 105 copies/mL.

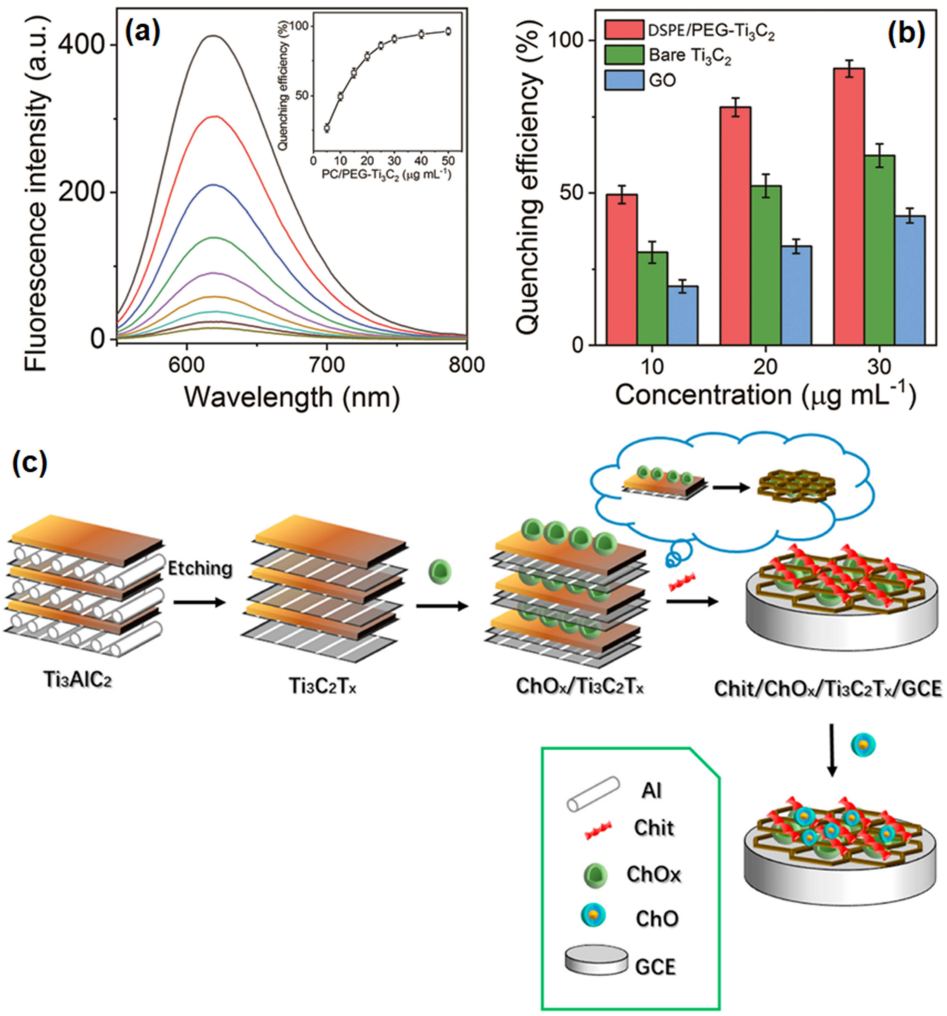

Figure 6 (**a**) Reduction of fluorescence intensity of RCDs on addition of Ti_3C_2 MXene, (**b**) quenching efficiency of different 2D materials Reprinted from[74] with permission, and (**c**) synthesis of the Chit/ChO_x/$Ti_3C_2T_x$/GCE Reprinted from[75] with permission.

Recently, a group of researchers has shown interest in creating MXene-based diagnostic probes for the detection of pathogenic bacteria. Zhang et al reported, for the first time, an MXene-based biosensing approach for *Mycobacterium tuberculosis* detection.[85] For developing the biosensor zirconium-linked Ti_3C_2 was used, and peptide nucleic acid (PNA)

Table 2 The Detection of Biomolecules and Pathogens by MXenes Based Biosensors

MXenes Materials	Target	LOD	Sensitivity	Ref
Chit/ChO_x/$Ti_3C_2T_x$/GCE	Cholesterol	0.12 nM	132.66 $\mu AnM^{-1}cm^{-2}$	[75]
$Ti_3C_2T_x$/GCE	DA	1 nM		[76]
Ti_3C_2/DNA/Pd/Pt@GCE	DA	27 nM		[77]
GOD_x/Au/MXene/Nafion/GCE	Glucose	2.6 μM	4.2 $\mu AmM^{-1}cm^{-2}$	[78]
AuNPs-PNA/target DNA/Ti_3C_2 MXene	*M tuberculosis*	20 CFU m/L		[70]
NH_2-pDNA/$Ti_3C_2T_x$	SARS-CoV-2	0.003 pM		[79]
ssDNA/$Ti_3C_2T_x$	SER-CoV-2 N gene	105 copies/mL		[80]
R6G-$Ti_3C_2T_x$@AuNRs-Ab2/ABEI	*Vibrio vulnificus*	10 CFU m/L-1 CFU m/L		[81]
$NiCo_2O_4$/Ti_2NbC_2	Glucose	0.298 mM	425.6 $\mu AmM^{-1}cm^{-2}$	[82]
P/T/Exo-III/Ti_3C_2 NS	HPV-18	100 pM		[83]

https://doi.org/10.2147/NSA.S580785

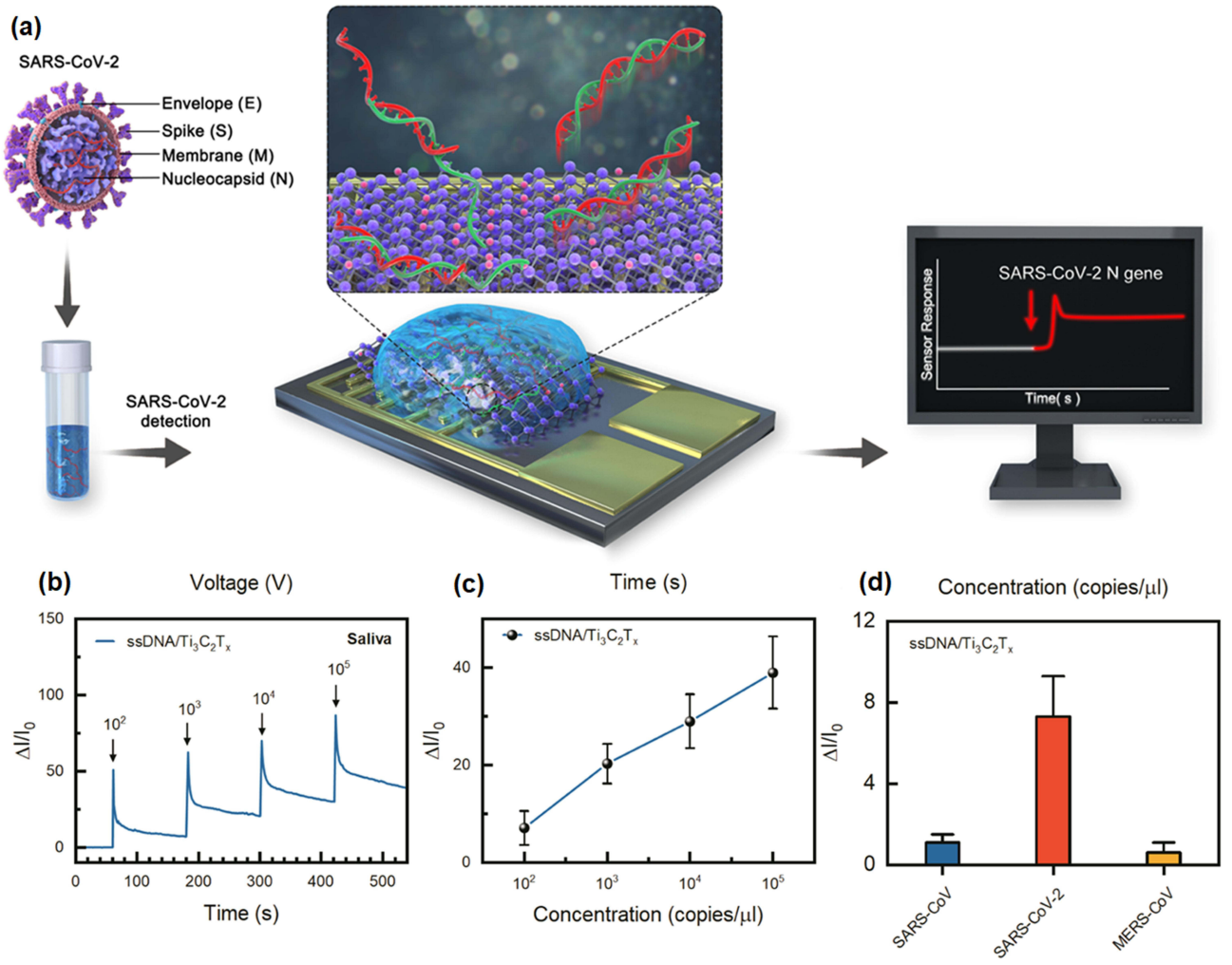

Figure 7 (**a**) Detection of SER-CoV-2 N gene by ssDNA/$Ti_3C_2T_x$ sensor, (**b**) Real-time response, (**c**) response versus concentration plot, and (**d**) selectivity test of ssDNA/$Ti_3C_2T_x$ sensor Reprinted from[80] with permission.

was used as the capture probe for targeting complementary biomarkers. This hybridized *M tuberculosis*-specific target biomarker was immobilized on the Au surface of the electrode, and accordingly, the conductance of this electrode was improved owing to the interaction between MXene and the target biomarkers. The advanced biosensor showed a high level of efficiency in detecting *S aureus, E coli, M smegmatis, P aeruginosa*, and the BCG vaccine.

Sensor for Food Contaminants

Various impurities, including gliotoxins, mycotoxins, endotoxins, exosomes, microorganisms, antibiotics, heavy metals, and pesticides are present in agricultural products. Mycotoxins can cause several health issues, including cancer and immune deficiency, which threaten both humans and animals. Similarly, another mycotoxin containing sulfur is gliotoxin, which belongs to a class of naturally occurring peptides generally known as piperazine-2,5-dione. It is regarded as one of the most toxic metabolites produced by certain species of fungi, such as *Aspergillus fumigatus*, and can cause significant environmental issues. A precise identification approach is essential to ensure food safety against gliotoxins and mycotoxins. Various traditional techniques, such as gas chromatography (GC), high-performance liquid chromatography (HPLC), and mass spectrometry, have been employed to detect food contaminants. However, these conventional methods have limitations, including the need for multiple assay steps, skilled personnel, and laborious pretreatments. Thus, there is a great need to develop fast, innovative, easy-to-use, sensitive, and stable detection methods to effectively identify mycotoxin contaminants. Therefore, MXene-based biosensors have been extensively investigated for the identification of

foodborne contaminants in the past decade.[86–89] Recently, researchers have concentrated on creating MXene-based biosensors to screen food contaminants. Aflatoxin (AF), which is found in various natural agricultural products, is a highly toxic mycotoxin known for its mutagenic, carcinogenic, and teratogenic properties.[90] The maximum permissible concentration of AFB1 in cereal products is 2.00 ppb, which is part of the total AF content of 4.0 ppb. Wu et al designed an SERS aptasensor specifically for AFB1 detection in agricultural foods.[91] The AFB1 aptamer was modified with Au nanoparticles (NPs), followed by the application of 4,40-Vinylenedipyridine as a trigger (Figure 8).AuNP/MXene SERS sensor was used to detect AFB1 in food products. Experimental findings indicated a LOD of 0.6 pg m/L and a linear concentration range of 1×10^{-3}–100 ng m/L. The formation of extensive SERS hot spots resulted from the hydrogen bonding between MXene and the aptamer.

Researchers have been interested in detecting T-2 toxins using nanomaterials such as CNTs, Au NPs, upconversion nanoparticles (UCNPs), and magnetic nanoparticles (MNPs). The complementary DNA (cDNA) was combined with MNPs, while the T-2 aptamer was paired with UCNPs to form a hybrid aptamer.[92] It has been noticed that with a decrease in the amount of T-2 antibodies, there was a decline in the electrochemical signal. The experimental findings demonstrated a strong response within the concentration range of 0.1–100 ng m/L for T-2 toxin. The recovered percentages obtained from the real samples using the developed sensor were found to be in the range of 95.97 to 104.00%. This result indicates that the proposed sensor has potential efficiency for the detection of T-2 toxins in food products.

Gliotoxin is another harmful metabolite found in some fungal species, such as *aspergillus fumigatus*, which poses significant risks to human and animal health. Wang et al examined a modified MXene-based DNA electrochemical biosensor for gliotoxin detection.[93] A chemical reaction involving the phosphate group of DNA and Ti was used to functionalize MXene nanosheets with tetrahedral DNA (TDNs). These modified DNA probes improved electron transfer between the electrochemical species and the electrode surface. Under optimized conditions, the proposed electrochemical

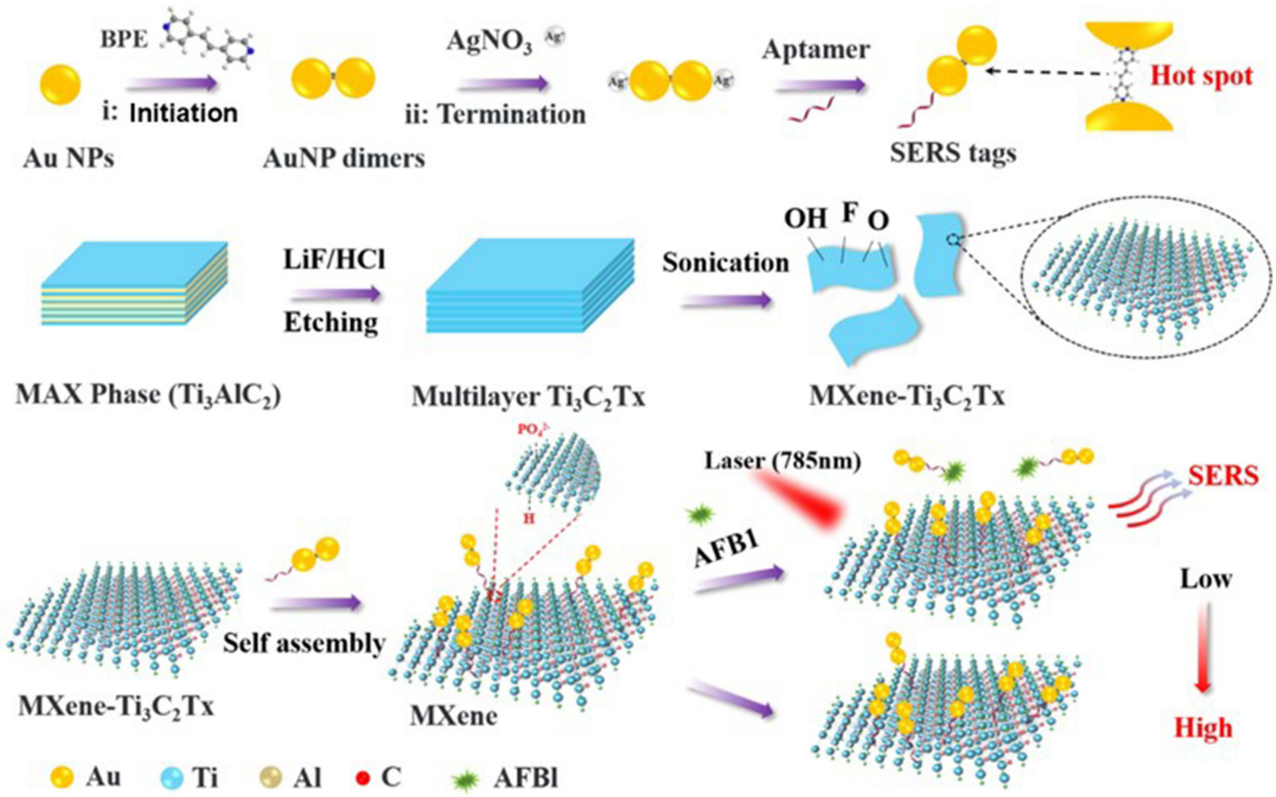

Figure 8 The AuNPs/Mxene SERS sensor for the detection of AFB1 contaminant in food i) Initiation: Start of formation of dimer, ii) Termination: End of formation of dimer.[88]

sensor exhibited a broad linear range of 5–10 nM and detection limit of 5 pM. The MXene-based electrochemical biosensor was evaluated using human serum with a satisfactory recovery of 96.3–115%.

Sensor for Environmental Pollutants

MXene nanostructures have recently gained significant attention for the detection of hazardous materials.[94] Liu et al were the first to report the detection of $NaNO_2$ using a MXene Ti_3C_2 composite.[95] This study demonstrated that Ti_3C_2 enabled electron flow in Hb, and provided a biosensor working within an extensive linear range of 0.5–11,800 μM for $NaNO_2$ detection with a detection limit of 0.12 μM. Organophosphate pesticides (OPs) are environmental pollutants frequently released into the atmosphere and that infiltrate agricultural operations. Song et al developed an innovative biosensor, AChEChit/Ti_3C_2/Au NPs/MnO_2/Mn_3O_4/GCE, for detecting OPs.[96] Under optimal conditions, this biosensor achieved impressive results and can detect at a low limit of 1.34×10^{-13} M. Additionally, the biosensor's capability to sense methamidophos in real samples was confirmed, exhibiting excellent recovery rates ranging from 95.2% to 101.3%.

Various MXene-based optical biosensors have been discussed in the literature for the detection of various metal ions through different mechanisms. Guan et al synthesized N-and P–modified Ti_3C_2, which showed a photoluminescence quantum yield (PLQY) of 20.1%.[97] These N/P@MQDs were utilized for the detection of Cu^{2+} ions. The photoluminescence (PL) intensity of the N/P@MQDs linearly decreased owing to FRET when Cu^{2+} ions were added in the range of 2–100 μM and 250–5000 μM, thus permitting the sensitive detection of Cu^{2+} at 2 μM. $Ti_3C_2T_x$ MQDs were also employed for the detection of Fe^{3+} ions.[92] The $Ti_3C_2T_x$ MQDs exhibited white, blue, and blue PL when prepared by the solvothermal method using ethanol, DMSO, and DMF, respectively. The PL QY (4.1, 10.7, and 6.9%) and the average size of the $Ti_3C_2T_x$ MQDs were also affected by the solvent selection. A range of ions, including Fe^{3+}, Fe^{2+}, Cu^{2+}, Ni^{2+}, Co^{2+}, Mn^{2+}, Ag^{+}, Al^{3+}, Cd^{2+}, Mg^{2+}, Hg^{2+}, Zn^{2+}, and Pb^{2+}, were used to evaluate the metal ion selectivity of the $Ti_3C_2T_x$ MQDs. The $Ti_3C_2T_x$ MQDs probe was found to detect Fe^{3+} within the linear ranges of 5–470 and 510–750 μM, with a minimum detection limit of 2 μM. Yang et al described Nb_2C MQDs for the detection of Fe^{3+} ions.[98] The PL intensity of the Nb_2C MQDs exhibited a linear quenching as the concentration of Fe^{3+} increased from 0 to 300 μM. This can be explained by the coordination relations between OH and –COOH surface groups on the Nb_2C MQDs and the Fe^{3+} ions. Rathi et al used water-soluble cationic surfactant cetyltrimethylammonium bromide (CTAB) during the exfoliation stage of Nb_2CT_x.[99] The modification with surfactant CTAB has shown a three times improvement in the NO_2 gas sensor. The gas sensor response increased from 0.543 ppm^{-1} to 1.686 ppm^{-1} upon modification with CTAB.

Hydrogen Production Using MXene

Hydrogen Production Using MXenes-Based Electrocatalysts

The growth of hydrogen energy is a practical solution to the current energy and environmental problems. An essential technique for hydrogen production via water splitting. MXene-based HER catalysts have attracted increasing interest in recent years. As HER electrocatalysts, MXenes and MXene-based composites exhibit encouraging developments as possible substitutes for Pt-based catalysts. 2D MXenes with -O/-OH groups showed metallic characteristics and confirmed their remarkable charge transfer capabilities.[100] The interaction between 2D MXenes and H was facilitated by these surface oxygen atoms. Further investigation revealed that the Heyrovsky mechanism was followed by HER for O-terminated MXenes. In terms of efficiency, the O-terminated surface outperformed the OH- and F-terminated surfaces. These findings show that terminated surface modifications can be beneficial for adjusting the catalytic activity of 2D MXenes in the HER.

Jiang et al used ultrathin O-functionalized Ti_3C_2 MXenes to create an efficient HER electrocatalyst.[101] Hydrogen adsorption kinetics were hindered by the F-functionalized MXenes on the basal plane, and adversely affected the HER. $Ti_3C_2T_x$ was dispersed in a KOH solution to create $Ti_3C_2O_x$, which reduced the F-termination through OH groups.[102] $Ti_3C_2(OH)_x$ was further calcined at 450°C in an Ar atmosphere, which caused a dehydration reaction, and the OH groups were converted to O-terminal groups. $Ti_3C_2O_x$ nanosheets have been demonstrated to be excellent HER electrocatalysts. Compared to $Ti_3C_2(OH)_x$, at a current density of 10 mA cm^{-2} $Ti_3C_2T_x$-450 exhibited an overpotential of 190 mV.

 https://doi.org/10.2147/NSA.S580785

Furthermore, the Tafel slope of 60.7 mV dec^{-1} is attributed to the highly active O sites on the basal plane of $Ti_3C_2O_x$. In conclusion, the terminal groups on the basal plane affect the catalytic efficiency of MXenes in the HER.

The HER activity of MXenes can be improved by confining them to single metal atoms. The stability of a single-atom catalyst in the 2D material lattice can be achieved through the formation of strong covalent bonds.[103] Using the model material Ti_3CNO_2, the influence of different metal atoms (Fe, Zn, Ir, Re, Os, and Rh) was examined in HER.[104] Additionally, Li et al demonstrated that the modification of MXenes with transition metal (TM) could enhance their catalytic performance.[105] The theoretical understandings of the catalytic mechanisms support the design and use of TM-doped MXenes in HER. Ultrathin 2D $Ti_{3-x}C_2T_y$ MXenes were used to produce $Pt_1/Ti_{3-x}C_2T_y$, a stable single-atom catalyst with a high reduction capacity and many Ti defect vacancies.[106] A single Pt atom MXene ($Mo_2TiC_2T_x$-Pt_{SA}) catalyst was formed by Zhang et al.[104] Double transition metal MXenes ($Mo_2TiC_2T_x$) were first exfoliated electrochemically, and then single Pt atoms were immobilized in the Mo vacancies (Figure 9). The $Mo_2TiC_2T_x$-Pt_{SA} performed better than pristine $Mo_2TiC_2T_x$ and $Mo_2TiC_2T_x$-V_{Mo} and achieved an overpotential of 30 mV at 10 mA cm^{-2}. Because of the strong interaction between the Pt atoms and $Mo_2TiC_2T_x$, $Mo_2TiC_2T_x$-Pt_{SA} exhibited exceptional stability as an HER electrocatalyst. Single-site Co-substituted 2D molybdenum carbide can be obtained from a Co-substituted Mo_2GaC MAX precursor.[107] At 10 mA cm^{-2} Mo_2CT_x:Co showed better activity than Mo_2CT_x with an overpotential of 180 mV. According to the DFT results, the co-substituted Mo_2CT_x improved the HER kinetics by increasing hydrogen adsorption on the MXene surface.

According to DFT calculations, hydrogen can be captured by the sides of MXene-containing metals and by C or N atoms. These species can act as fast-moving reaction sites for the evolution of hydrogen. The creation of particular nanostructures is a creative way to improve the HER activity of MXene. MXene nanoribbons or nanodots can be prepared using a variety of synthetic techniques, such as ball-milling[109] and hydrothermal treatment.[110] HF etching can also be used to produce $Ti_3C_2T_x$ nanofibers (NFs) from hydrolyzed Ti_3AlC_2.[111] With an overpotential of 169 mV at 10 mA cm^{-2}, the resultant $Ti_3C_2T_x$ NFs performed better than $Ti_3C_2T_x$ flakes, which had an overpotential of 385 mV. Furthermore, the specific surface area and number of active sites of MXene NFs were far greater than those of MXene flakes. Consequently, the exceptionally high HER performance of the $Ti_3C_2T_x$ NFs can be attributed primarily to the enhancement of the specific surface area and the large number of active sites.

The combination of MXenes with various active materials, including chalcogenides,[112] layered hydroxides,[113] phosphides,[114] metal nanoparticles,[115] and metal-free black phosphorus,[116] has shown enhanced HER activity. Following freezing with liquid nitrogen and subsequent annealing, a hierarchical $MoS_2/Ti_3C_2T_x$ structure was achieved.[117] The rapid freezing process facilitated the rolling of the $Ti_3C_2T_x$ nanowires and the formation of vertically aligned MoS_2 microcrystals. The $MoS_2/Ti_3C_2T_x$ composite offered numerous active sites for electrocatalytic processes

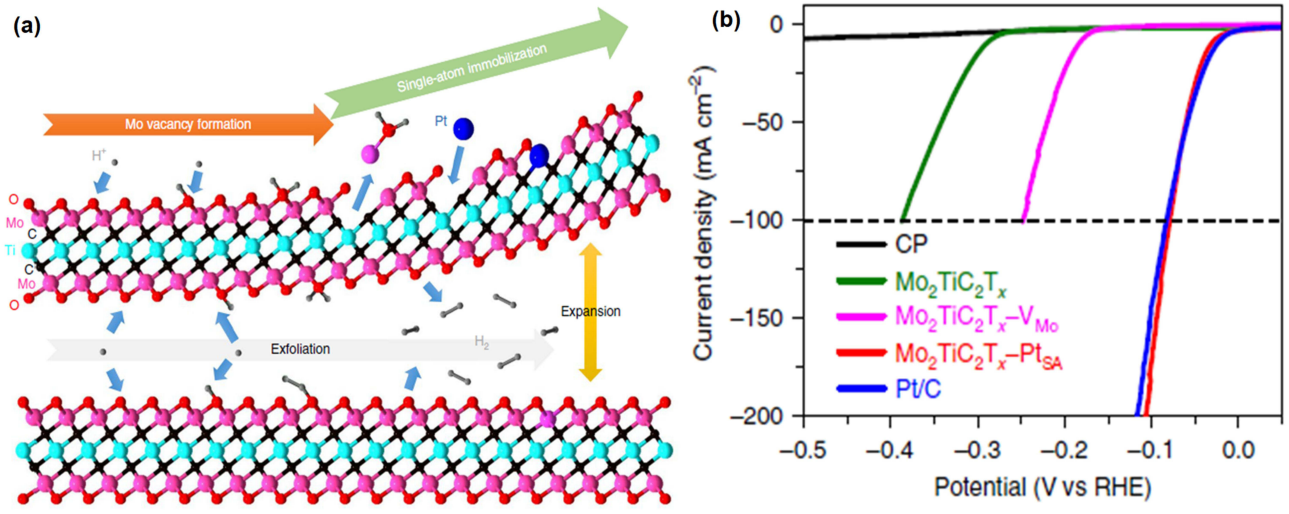

Figure 9 (**a**) Synthesis of $Mo_2TiC_2T_x$-Pt_{SA}, (**b**) Polarization curve during HER Reprinted from[108] with permission.

and enhanced the charge transfer. The catalytic performance was excellent, with an initial overpotential of 30 mV and low overpotential of 168 mV at 10 mA cm^{-2}. Furthermore, the exchange current density was improved more than 25 times. By placing several carbon-coated MoS_2 nanocrystals on carbon-stabilized Ti_3C_2 MXenes, a new composite material $MoS_2/Ti_3C_2T_x$@C was prepared.[118] The resulting nanocrystal material exhibited exceptional HER activity and constancy in acidic environments. In addition to MoS_2, other transition metal chalcogenides, such as NiS_2,[119] VS_2,[120] and $MoSe_2$,[121] in combination with MXenes can improve HER activity. MXene-supported metal nanoparticles (NPs) can significantly enhance HER activity. Li et al described the presence of Pt_3Ti NPs on $Ti_3C_2T_x$ MXenes, where Pt interacted with Ti through in-situ co-reduction.[122] As the temperature increased, Pt atoms were converted to intermetallic compounds, as observed from the in-situ X-ray absorption spectra $Pt/Ti_3C_2T_x$-550 exhibited excellent performance, and a mere 32.7 mV potential was required at 10 mA cm^{-2}. Wang et al developed a new composite, FeNi@$Mo_2TiC_2T_x$ @Ni foam (NF), by incorporating Fe^{2+} ions and subsequent in situ coupling with surface Ni atoms on nickel foam.[123] FeNi@$Mo_2TiC_2T_x$@NF displayed high HER activity with an overpotential of 165 mV at 10 mA cm^{-2}, which is attributed to the synergistic effect of $Mo_2TiC_2T_x$ and FeNi nanoalloys.

MXenes-Based Photocatalysts for Hydrogen Production

Remarkable electrical conductivity, high surface area, and variable surface functionality are some of the key factors contributing to the promising activity of MXene-based materials in photocatalytic hydrogen evolution reactions. These properties can improve the charge separation and electron flow in the photocatalysts. After combining with semiconductors, such as TiO_2, g-C_3N_4, or metal sulfides, MXenes promote the effective absorption of light and electron flow. Additionally, strong interfacial bonding with other photocatalytic materials is made possible by their surface functional groups, which increase photocatalytic activity. Table 3 presents various 2D MXene-based photocatalytic systems and their hydrogen production activities.

To increase the efficiency of hydrogen production, Chen et al created a CdS NS@Ti_3C_2 MXene composite using a one-step solvothermal method.[139] CdS NS@Ti_3C_2 exhibited the best photocatalytic performance and achieved a hydrogen evolution rate of 1.73 mmol g^{-1} h^{-1}, which is almost five times higher than that of CdS nanosheet. UV–vis DRS analysis of the composite material indicated improved light absorption owing to the addition of Ti_3C_2 MXene. Photoluminescence (PL) and time-resolved PL analyses showed that the carrier lifetime of CdS NS@Ti_3C_2-5 was longer than that of CdS NS. The apparent quantum efficiency (AQE) showed a maximum value of 9.56% when irradiated with light at 370 nm. This result highlights the collaborative effect of 2D CdS and Ti_3C_2 MXene, which enhances the effective

Table 3 Photocatalytic Hydrogen Production Activity by Various MXenes Based Catalysts

MXenes Based Catalyst	H_2 Evolution Rate (μmol h^{-1} g^{-1})	Ref
$CdS/Ti_3C_2T_x$	84500	[124]
$CdS/Ti_3C_2T_x$	14342	[125]
CdS/Nb_2CT_x	5040	[126]
$V_2C/g\text{-}C_3N_4$	360000	[127]
g-C_3N_4@Ti_3C_2 QDs	5111.2	[128]
g-C_3N_4/p-$Ti_3C_2T_x$	982	[129]
g-$C_3N_4/Ti_3C_2T_x$/Pt	1948	[130]
Ti_3C_2@TiO_2@MoS_2	6425	[131]
PtO/ Ti_3C_2/TiO_2-600	11,412	[132]
$CuZnInS/Ti_3C_2$	15240	[133]
MoS_2/Ti_3C_2	6144.7	[134]
TiO_2/Fe_2O_3@Ti_3C_2	1634.64	[135]
$SnS_2/Ti_3C_2/TiO_2$	10,505.8	[136]
MXene–CdS/WO_3	27,500	[137]
TiO_2/Ti_3C_2/g-C_3N_4	1150	[138]

https://doi.org/10.2147/NSA.S580785

transfer of photogenerated charges and significantly increases hydrogen production in the absence of metal co-catalysts. Similarly, Huang et al developed a $Ti_3C_2T_x$ MXene/CdS (CMX) composite through the in situ growth of CdS nanosheets on exfoliated $Ti_3C_2T_x$ via a solvothermal approach.[124] The optimized catalyst (CM3, containing 3% MXene) exhibited a hydrogen production rate of 28.7 mmol g^{-1} h^{-1} under visible light irradiation. This heterojunction showed 4.2 times higher activity compared to pure CdS (6.9 mmol g^{-1} h^{-1}) and 26 times higher activity relative to the Pt-loaded CdS (11.2 mmol g^{-1} h^{-1}). Moreover, the CM3 catalyst exhibited excellent recyclability over four consecutive cycles. This enhanced reactivity is due to synergies, improved light absorbability, Schottky-type charge separation, and solvothermal effects.

Modification of surface terminations greatly enhances photocatalytic hydrogen evolution using MXene-based catalysts. Ran et al developed a CdS/Ti_3C_2 photocatalyst using a hydrothermal method to substitute expensive Pt with more abundant co-catalysts for hydrogen production through a photocatalytic process.[125] The surface of Ti_3C_2 was modified by introducing –O and –OH groups to prepare a CdS/Ti_3C_2 heterojunction photocatalyst. It showed an impressive hydrogen production of 14,342 μmol g^{-1} h^{-1} under visible-light irradiation, which is higher than that of the 2.5 wt% Pt-loaded CdS. During the hydrothermal process, the-F terminations of Ti_3C_2 were substituted by -OH and -O groups. This modification increased the number of active sites -O functional groups and enhanced the efficiency of MXenes for the HER.

Wang et al explain the synthesis of a 2D/3D CdS nanoflowers/Ti_3C_2 MXene heterostructures and its photocatalytic hydrogen evolution efficiency.[140] Utilizing 0.25 M Na_2S and 0.35 M Na_2SO_3 in water as the sacrificial solution, the hydrogen generation rate of 15 wt% Ti_3C_2/CdS under visible light irradiation reached at 88.162 mmol g^{-1} h^{-1}. Integrated lamellar Ti_3C_2 MXene enhances the separation efficiency of photogenerated carriers and improves light absorption owing to the integration of the 2D and 3D structures. This composite promoted swift electron flow from the CdS to the Ti_3C_2 layers, which minimized charge recombination. Xiao and Zhang prepared a 1D/2D CdS/Ti_3C_2 composite through the growth of CdS nanorods on Ti_3C_2.[141] This nanocomposite, containing 20 mg of MXene, demonstrated notable photocatalytic hydrogen generation of 2407 μmol g^{-1} h^{-1} under visible light irradiation. This enhanced photoactivity is due to the distinctive 2D structure, high electrical conductivity, and superior light-harvesting ability of Ti_3C_2. In a similar manner, Ding et al employed a series of electrostatic self-assembly processes and a solvothermal technique to produce 2D/2D CdS/$Ti_3C_2T_x$ composites and examined their photocatalytic hydrogen evolution.[142] The resulting photocatalyst achieved a hydrogen evolution rate of 3226 μmol g^{-1} h^{-1} when lactic acid was used as the sacrificial chemical (Figure 10).

The work presented by Huang et al illustrated the in situ formation of a 1D CdS/2D Nb_2CT_x MXene Schottky heterojunction to enhance photocatalytic hydrogen generation.[126] In this respect, the solvothermal method was adopted to ensure strong interfacial contact between CdS nanorods and Nb_2CT_x MXene nanosheets. This arrangement promotes efficient charge separation, which is essential for the photocatalytic processes. The optimized CdS/Nb_2CT_x composite showed a hydrogen production rate of 5040 μmol g^{-1} h^{-1} when exposed to visible light irradiation. This heterojunction shows an enhancement of about 4.3 times in hydrogen production activity over pristine CdS nanosheets. This enhancement in performance is due to the formation of a Schottky heterojunction between CdS and Nb_2CT_x. In addition, Nb_2CT_x MXene controls the agglomeration of the CdS nanorods, thus maintaining a high surface area that promotes catalysis.

Sherryna et al explored a V_2C MXene/g-C_3N_4 nanocomposite as an effective photocatalyst for hydrogen evolution under visible-light irradiation.[127] The optimal composite containing 15 wt% vanadium carbide (V_2C) exhibited a hydrogen production rate of 360 mmol g^{-1} h^{-1}, almost four times greater than that of g-C_3N_4. The strong interaction between the two surfaces and the Schottky barrier formed at the V_2C/g-C_3N_4 interface facilitated charge separation and delayed recombination. The group tested various sacrificial solvents, including methanol, glycerol, and Triethanolamine (TEOA), for their effects on the photocatalytic activity. Methanol, which acts as a sacrificial reagent, produces the maximum amount of hydrogen, followed by TEOA. This observation indicates that sacrificial reagents can significantly enhance catalytic activity and directly influence the photoredox reaction as h+ scavengers.

Li et al developed g-C_3N_4@Ti_3C_2 quantum dots (QDs) using a self-assembly method and examined their photocatalytic hydrogen generation capabilities.[128] An ideal photocatalyst with 100 mL Ti_3C_2 MXene QDs exhibited a remarkable photocatalytic hydrogen generation rate of 5111.8 μmol g^{-1} h^{-1}. This remarkable performance was due to the enhanced specific surface area of g-C_3N_4, increase in the number of active sites, and enhanced electronic conductivity of the composite material.

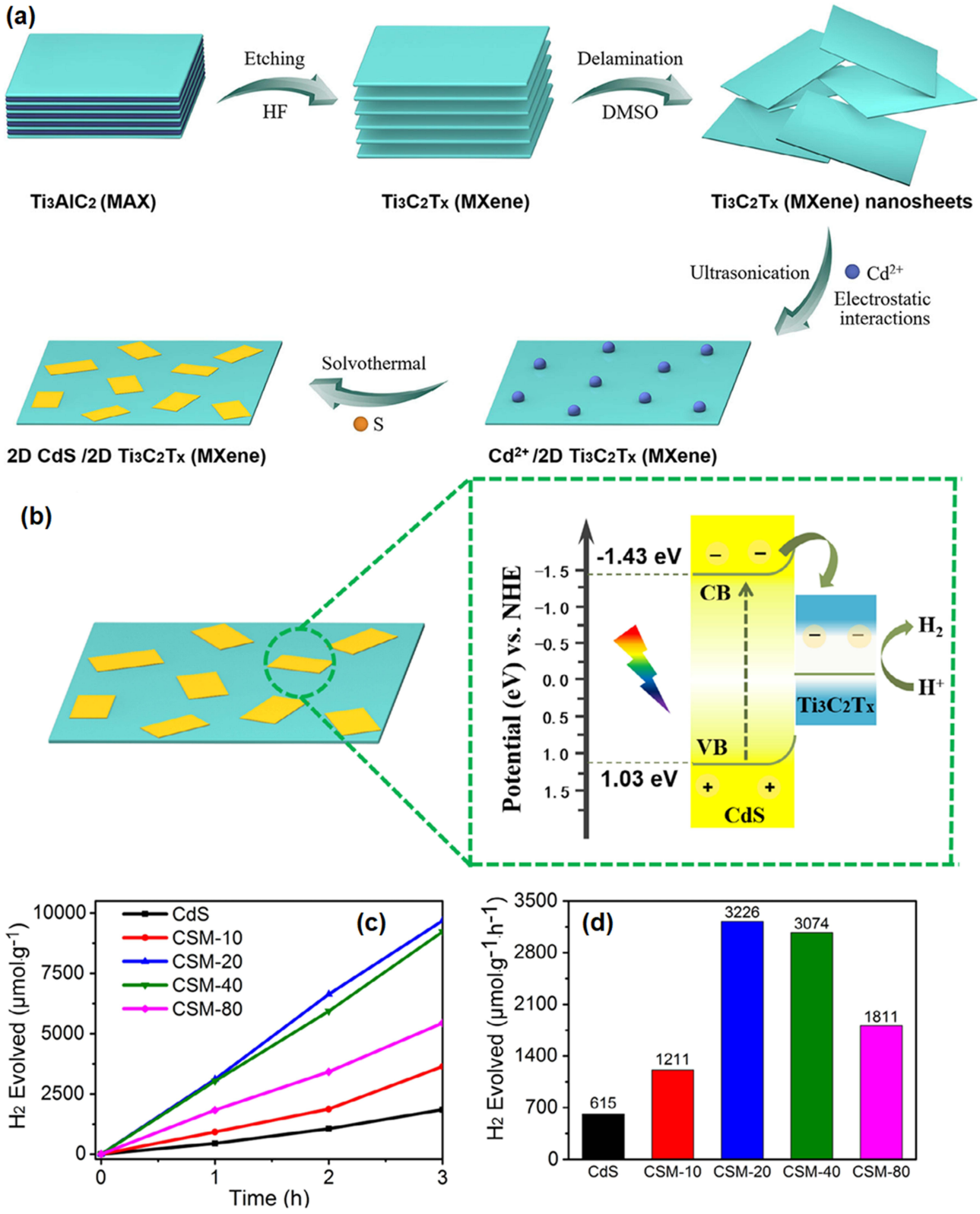

Figure 10 (**a**) Preparation of CdS/$Ti_3C_2T_x$ composites, (**b**) Mechanism for H_2 generation, and Photocatalytic activity for H_2 generation (**c** and **d**) Rainbow arrow: Visible light, Dashed arrow: Transition of electron from VB to CB Reprinted from[126] with permission.

https://doi.org/10.2147/NSA.S580785

Wong et al developed a crystalline g-C_3N_4/$Ti_3C_2T_x$ MXene by integrating $Ti_3C_2T_x$ MXene in crystalline g-C_3N_4 through a combined salt-assisted and freeze-drying method to enhance the photocatalytic production of H_2.[143] The ideal photocatalyst g-C_3N_4/$Ti_3C_2T_x$/Pt (0.5 wt% $Ti_3C_2T_x$) achieved a H_2 generation rate of 2651.93 μmol g^{-1} h^{-1}. The authors explained that the enhanced performance is due to the synergistic effect of the strongly crystalline phase of g-C_3N_4, which promotes rapid charge mobility, along with the strong role of the dual co-catalysts $Ti_3C_2T_x$ and Pt, which enhances the charge separation efficiency and produces numerous active sites. In general, g-C_3N_4/$Ti_3C_2T_x$ composites without co-catalyst Pt exhibited lower photocatalytic activities than those of the g-C_3N_4-MXene system with Pt. For example, g-C_3N_4/p-$Ti_3C_2T_x$ synthesized by Kang et al[129] showed a hydrogen generation rate of 982.2 μmol g^{-1} h^{-1}, whereas a higher photocatalytic hydrogen evolution rate of 1948 μmol g^{-1} h^{-1} was reported for g-C_3N_4/$Ti_3C_2T_x$/Pt synthesized by Liu et al.[130]

Li et al described the synthesis of an innovative photocatalyst composed of Ti_3C_2 MXene, MoS_2, and TiO_2 nanosheets (Figure 11).[131] This ternary heterostructure showed a remarkable improvement in photocatalytic hydrogen generation under simulated sunlight irradiation compared with its individual and binary analogs. This improvement was due to the effective charge pair separation and transport resulting from the closely packed 2D–2D interface, high surface area, and more active sites from TiO_2. A further increase in the hydrogen evolution rate of 6425.30 μmol h^{-1} g^{-1} was demonstrated by the ideal composite (Ti_3C_2@TiO_2@MoS_2 with 15 wt% MoS_2) compared to TiO_2 and the composite Ti_3C_2@TiO_2. This study outlined the synergistic effect of the three constituents, where Ti_3C_2 acted as an electron pool, MoS_2 served as a co-catalyst that reduced the overpotential, and TiO_2 was the primary light absorber.

To increase the efficiency of photocatalytic hydrogen evolution using Ti_3C_2 MXene-based materials, a new PtO/Ti_3C_2/TiO_2 ternary composite was synthesized using an in-situ oxidation and photodeposition process by Yang et al.[132] Firstly, Ti_3C_2 MXene was oxidized thermally to form a Ti_3C_2/TiO_2 heterojunction, and then PtO nanodots were deposited to improve catalytic performance. Among the prepared materials, the PtO/Ti_3C_2/TiO_2-600 demonstrated the highest hydrogen generation compared to Ti_3C_2/TiO_2-600 without PtO. Sun et al prepared a highly effective and stable CuZnInS/Ti_3C_2 catalyst for hydrogen production.[133] The improvement in catalytic activity is attributed to the effective inhibition of charge-carrier recombination due to the presence of MXene. The application of co-catalysts is a well-established approach for enhancing the activity of photocatalysts. M Shao et al reported that MoS_2/Mo_2C acted as a highly effective co-catalyst for photocatalytic hydrogen generation.[144] The CdS-based catalyst, which was modified by

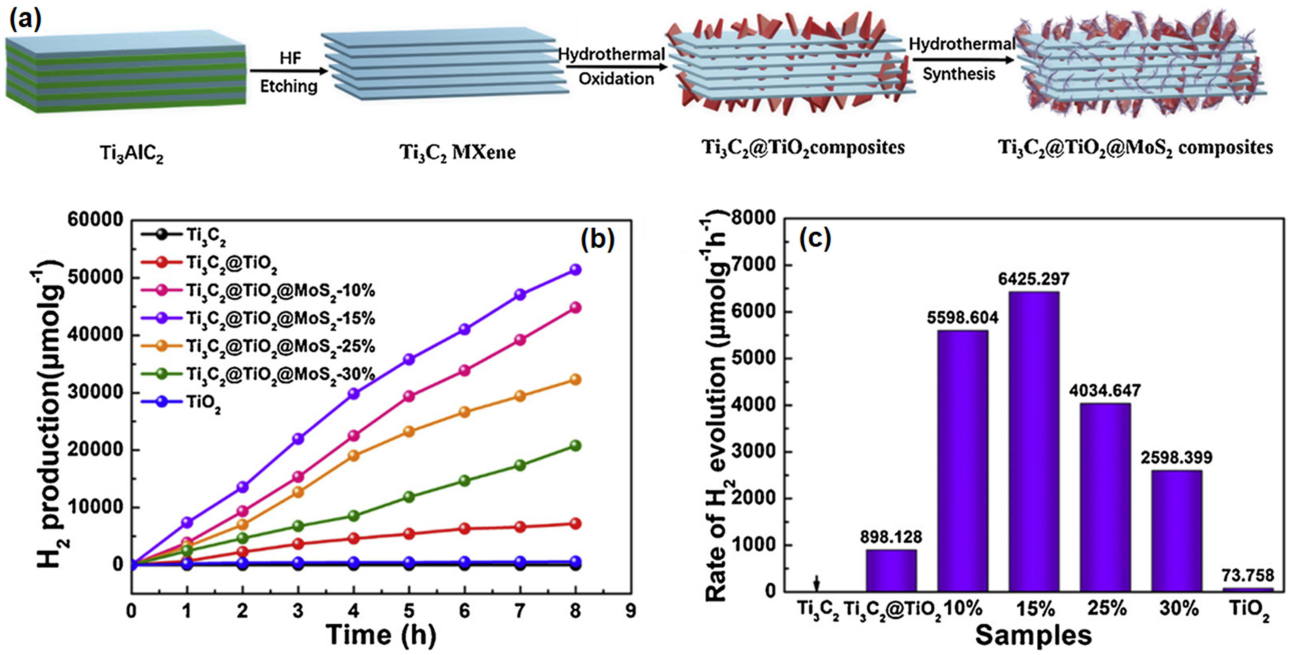

Figure 11 (**a**) Synthesis of Ti_3C_2@TiO_2@MoS_2, (**b**) Photocatalytic hydrogen production with time, (**c**) Comparison of photocatalytic hydrogen production rate of different composites Reprinted from[131] with permission.

https://doi.org/10.2147/NSA.S580785

integrating MoS_2/Mo_2C, has significant results in photocatalytic hydrogen evolution and showed a remarkably high rate of 34,000 μmol $g^{-1}h^{-1}$, which is nearly 112 times higher than that of pure CdS.

Density Functional Theory (DFT) Modeling of HER Activity in MXenes

DFT modeling is significantly important for predicting the HER activity of MXenes by studying the influence of terminal surface functional groups on electronic structure and adsorption characteristics. The Gibbs free energy of hydrogen adsorption (ΔG_{H*}) is commonly applied as an activity descriptor for the hydrogen evolution reaction.[145]

$$\Delta G_{H*} = \Delta E_{ads} + \Delta E_{ZPE} + T\Delta S$$

where ΔE_{ads} and ΔE_{ZPE} indicate the adsorption energy and zero-point energy correction based on DFT calculations, T and ΔS represent the temperature and the entropy change. Near-zero values for this parameter ensure optimized HER activity. DFT predictions always show that the terminated surfaces containing –O and –OH groups affect the d-band center of transition metals present in MXenes. As a result, favorable hydrogen binding is observed compared to MXenes terminated by -F groups, which decrease the HER activity by exhibiting unfavorable electronic interactions.[146] Predicted DFT values for terminated surfaces containing varying amounts of ΔG_{H*} are in good agreement with experimentally measured values for obtained overpotentials and Tafel slopes on MXene surfaces.[146] Thus, DFT modeling serves as a vital bridge between theory and experiment for balanced MXene-based HER catalyst design.

Stability of MXenes-Based Materials

MXenes have drawn rapidly growing interest in biosensing and catalysis for their remarkable properties, but their poor oxidation stability remains a critical limitation to their practical implementation in aqueous and ambient environments.[147] In water and moist air, MXenes undergo gradual oxidation, forming TiO_2, amorphous carbon, or gaseous byproducts, which reduces the conductivity, structural integrity, and catalytic activity.[148,149] Recent studies have shown that such oxidation is highly site-specific, starting preferentially at flake edges, defect-rich regions, and undercoordinated Ti sites where water and dissolved oxygen readily adsorb. Lipatov et al observed that the oxidation of MXene initiates at the edges, where there are completely uncovered areas that are exposed to oxidizing substances.[149] Hydrolysis-driven pathways have increasingly been recognized as dominant under ambient conditions, often offsetting the role of molecular oxygen alone.[150,151] For the first time, the water-induced degradation of MXenes was studied by Wu et al in 2022.[151] They performed a first-principle molecular dynamics (FPMD) simulation, and the results indicated that the interaction of water molecules with the basal plane of the MXene happens simultaneously with the breaking of the bonds between titanium and the MXene sheets. Water molecules irreversibly adsorbed on the surface of Ti atoms, deprotonated it and pullout Ti atoms. To mitigate degradation, several stabilization strategies have been developed, including antioxidant capping using ascorbates or polyphenols that covered surface Ti atoms and suppress water attack, as well as edge passivation via polyanions or surfactants.[152] Inert or low-temperature storage, high-concentration dispersions, and controlled pH environments further extend MXene shelf-life. These advances are essential for improving MXene biocompatibility, preserving catalytic longevity, and enabling consistent performance in real-world aqueous applications.

Conclusion and Future Perspective

MXenes have seen major breakthroughs owing to their uniqueness in being as two-dimensional material, high hydrophilicity, high electrical conductivity, large potential for surface modification, high malleability, and ion insertion. With scientists investigating further into finding new uses for MXene in different domains of science, major advancements have been made in the development of supercapacitors for holding chemical energy. This review article aims to cover the structure, properties, preparation methods, and applications of MXene-based composites in developing biosensors and hydrogen production, covering recent studies on various composites of MXene. Presently, the major methods of MXene preparation are through etching, which can be either acidic or alkaline, and have mostly focused on HF etching. This method presents a major hazard with regard to the use of highly corrodible substances such as waste acids and bases. These traditional methods, besides being harmful to the environment, involve low mass production and incur major costs.

Although direct preparation methods involve advancements in finding ways to synthesize MXenes without releasing toxic substances, there is still a major need for advancements in their production efficiency. Hence, there is a major urgency to develop a novel method of MXene preparation, which would help in scaling up their manufacturing.

Currently, MXenes are considered some of the most promising materials owing to their numerous applications, including environmental monitoring, biosensing, and health monitoring. They are especially well suited for biosensing because of their remarkable physicochemical characteristics, including excellent electrical conductivity, biocompatibility, and surface modifications. In this review, a critical overview of the recent advances in MXene-based biosensors is presented. Even with this promising development, issues that need to be considered include enhancement in large-scale production, reproducibility, and biocompatibility of MXene-based biosensors with reduced toxicity and ensuring their long-term stability. A major challenge is the scalability of MXene-based biosensors for industrial manufacturing. Further studies are needed to enhance the reproducibility of these sensors in practical applications and ensure consistency across batches. In this review, recent developments in the use of MXenes as electrocatalysts for HER are discussed. Although MXene-based electrocatalysts have been greatly improved in recent decades, it is still challenging to produce highly active electrocatalysts that can outperform Pt-based materials and be commercialized. These materials offer excellent solar energy absorption and conversion capabilities for the production of hydrogen. The overall photocatalytic performance of MXenes increases with enhanced light absorption, effective charge carrier separation, and enhanced surface reactions upon coupling with other semiconductors.

Recent advancements in MXene-based nanomaterials have shown great potential in the design of photocatalytic semiconductors; however, the journey to establish stable nanocatalysts is long. Although these nanomaterials hold incredible promise, they must undergo deep ecotoxicological assessments and life-cycle evaluations before further applications. Future studies related to kinetics and thermodynamic control technologies involved in the synthesis of MXene-based photocatalysts should be conducted. With the high photocatalytic efficiency of the removal of organic pollutants in water, it is possible to expect that MXene-based composite photocatalysts will also successfully serve in the case of air pollutants, such as volatile organic compounds, NO, SO_2, H_2S, NO_2, and various exhaust emissions.

Acknowledgments

ASR acknowledges the Royal Society, UK, for its Newton International Alumni Fellowship Fund, and Woxsen University.

Author Contributions

All authors made a significant contribution to the work reported, whether that is in the conception, study design, execution, acquisition of data, analysis and interpretation, or in all these areas; took part in drafting, revising or critically reviewing the article; gave final approval of the version to be published; have agreed on the journal to which the article has been submitted; and agree to be accountable for all aspects of the work.

Disclosure

The authors report no conflicts of interest in this work.

References

1. Huang X, Tan CL, Yin ZY, Zhang H. Hybrid nanostructures based on two-dimensional nanomaterials. *Adv Mater*. 2014;26:2185–2204. doi:10.1002/adma201304964
2. Torrisi F, Coleman JN. Electrifying inks with 2D materials. *Nat Nanotechnol*. 2014;9:738. doi:10.1038/nnano2014218
3. Liu L, Park J, Siegel DA, et al. Heteroepitaxial growth of two-dimensional hexagonal boron nitride templated by graphene edges. *Science*. 2014;343:163–167. doi:10.1126/science1246137
4. Bao X, Ou Q, Xu ZQ, Zhang Y, Bao Q, Zhang H. Band structure engineering in 2D materials for optoelectronic applications. *Adv Mater Technol*. 2018;3:1800072. doi:10.1002/admt201800072
5. Ida S, Ogata C, Eguchi M, Youngblood WJ, Mallouk TE, Matsumoto Y. Photoluminescence of perovskite nanosheets prepared by exfoliation of layered oxides, $K_2Ln_2Ti_3O_{10}$, $KLnNb_2O_7$, and $RbLnTa_2O_7$ (Ln: lanthanide ion). *J Am Chem Soc*. 2008;130:7052–7059. doi:10.1021/ja7114772
6. De S, Acharya S, Sahoo S, Shim JJ, Nayak GC. From 0D to 3D MXenes: their diverse syntheses, morphologies and applications. *Mater Chem Front*. 2022;6:818–842. doi:10.1039/D2QM00002D

7. Naguib M, Kurtoglu M, Presser V, et al. Two-dimensional nanocrystals produced by exfoliation of Ti_3AlC_2. *Adv Mater*. 2011;23:4248–4253. doi:10.1002/adma201102306
8. Gogotsi Y, Anasori B. The rise of MXenes. *ACS Nano*. 2019;13:8491–8494. doi:10.1021/acsnano9b06394
9. Liu Z, Zheng L, Sun L, Qian Y, Wang J, Li M. $(Cr_{2/3}Ti_{1/3})_3AlC_2$ and $(Cr_{5/8}Ti_{3/8})_4AlC_3$: new MAX-phase compounds in Ti-Cr-Al-C system. *J Am Ceram Soc*. 2013;97:67–79. doi:10.1111/jace12731
10. Otgonbayar Z, Yang S, Kim IJ, Oh WC. Recent advances in 2D MXene and solid state electrolyte for energy storage applications: comprehensive review. *Chem Eng J*. 2023;472:144801. doi:10.1016/jcej2023144801
11. Lorencova L, Kasak P, Kosutova N, et al. MXene-based electrochemical devices applied for healthcare applications. *Microchim Acta*. 2024;191:88.
12. Iqbal A, Kwon J, Kim MK, Koo CM. MXenes for electromagnetic interference shielding: experimental and theoretical perspectives. *Mater Today Adv*. 2021;9:100124–100139. doi:10.1016/jmtadv2020100124
13. Sezen S, Zarepour A, Zarrabi A, Iravani S. MXene-based biosensors for selective detection of pathogenic viruses and bacteria. *Microchem J*. 2023;193:109258. doi:10.1016/jmicroc2023109258
14. Zhang Q, Wang F, Zhang H, Zhang Y, Liu M, Liu Y. Universal Ti_3C_2 MXenes based self-standard ratiometric fluorescence resonance energy transfer platform for highly sensitive detection of exosomes. *Anal Chem*. 2018;90:12737–12744. doi:10.1021/acsanalchem8b03083
15. Khorsandi D, Yang JW, Ulker Z, et al. MXene-based nano(bio)sensors for the detection of biomarkers: a move towards intelligent sensors. *Microchem J*. 2024;197:109874. doi:10.1016/jmicroc2023109874
16. Tian S, Wang M, Fornasiero P, et al. Recent advances in MXenes-based glucose biosensors. *Chin Chem Lett*. 2023;34:108241. doi:10.1016/jcclet2023108241
17. Iravani S, Varma RS. MXenes in cancer nanotheranostics. *Nanomaterials*. 2022;12:3360. doi:10.3390/nano12193360
18. Abdulwahid FS, Haider AJ, Al-Musawi S. Folate decorated dextran-coated magnetic nanoparticles for targeted delivery of ellipticine in cervical cancer cells. *Adv Nat Sci Nanosci Nanotechnol*. 2023;14:015001. doi:10.1088/2043-6262/aca606
19. Yoon J, Shin M, Lim J, Lee JY, Choi JW. Recent advances in MXene nanocomposite-based biosensors. *Biosensors*. 2020;10:185. doi:10.3390/bios10110185
20. Hadi AJ, Nayef UM, Mutlak FA-H, Jabir MS, Muayad MW. Antibacterial and anticancer properties of zinc oxide nanoparticles: a review of current advances and future directions. *J Appl Sci Nanotechnol*. 2025;5:60. doi:10.53293/jasn202575411330
21. Tian L, Qi J, Ma X, et al. A facile DNA strand displacement reaction sensing strategy of electrochemical biosensor based on n-carboxymethyl chitosan/molybdenum carbide nanocomposite for microrna-21 detection. *Biosens Bioelectron*. 2018;122:43–50. doi:10.1016/jbios201809037
22. Yuan X, Zhang M, Wu Y. MXene-based sensors for detecting human physiological information. *Sens Mater*. 2020;32:4047–4065.
23. Rasool K, Helal M, Ali A, Ren CE, Gogotsi Y, Mahmoud KA. Antibacterial activity of $Ti_3C_2T_x$ MXene. *ACS Nano*. 2016;10:3674–3684. doi:10.1021/acsnano6b00181
24. Dwivedi N, Dhand C, Kumar P, Srivastava AK. Emergent 2D materials for combating infectious diseases: the potential of mxenes and mxene-graphene composites to fight against pandemics. *Mater Adv*. 2021;2:2892–2905. doi:10.1039/D1MA00003A
25. Li Y, Peng Z, Holl NJ, et al. MXene-graphene field-effect transistor sensing of influenza virus and SARS-CoV-2. *ACS Omega*. 2021;6:6643–6653. doi:10.1021/acsomega0c05421
26. Kumar S, Lei Y, Alshareef NH, Quevedo-Lopez MA, Salama KN. Biofunctionalized two-dimensional Ti_3C_2 MXenes for ultrasensitive detection of cancer biomarker. *Biosens Bioelectron*. 2018;121:243–249. doi:10.1016/jbios201808076
27. Rhouati A, Berkani M, Vasseghian Y, Golzadeh N. MXene-based electrochemical sensors for detection of environmental pollutants: a comprehensive review. *Chemosphere*. 2022;291:132921. doi:10.1016/jchemosphere2021132921
28. Janjhi FA, Ihsanullah I, Bilal M, Castro-Munoz R, Boczkaj G, Gallucci F. MXene-based materials for removal of antibiotics and heavy metals from wastewater—a review. *Water Resour Ind*. 2023;29:100202. doi:10.1016/jwri2023100202
29. Gopalram K, Kapoor A, Kumar PS, Sunil A, Rangasamy G. MXenes and MXene-based materials for removal and detection of water contaminants: a review. *Ind Eng Chem Res*. 2023;62:6559–6583. doi:10.1021/acsiecr3c00595
30. Zahra QUA, Ullah S, Shahzad F, et al. MXene-based aptasensors: advances, challenges, and prospects. *Prog Mater Sci*. 2022;129:100967.
31. Otgonbayar Z, Oh WC. Comprehensive and multi-functional MXene-based sensors: an updated review. *Flatchem*. 2023;40:100524. doi:10.1016/jflatc2023100524
32. Zubair M, Hassan MMU, Mehran MT, Baig MM, Hussain S, Shahzad F. 2D MXenes and their heterostructures for HER, OER and overall water splitting: a review. *Int J Hydrogen Energy*. 2022;47:2794–2818. doi:10.1016/jijhydene202110248
33. Hou L, Peng X, Lyu S, et al. Advancements in MXene-based nanohybrids for electrochemical water splitting. *Chin Chem Lett*. 2024;110392.
34. Tripathy DB. Applications of MXenes in hydrogen evolution/oxygen evolution and nitrogen reduction reactions. *Sustain Energy Fuels*. 2024;8:3801–3828. doi:10.1039/D4SE00556B
35. Sinha A, Dhanjai, Zhao H, et al. MXene: an emerging material for sensing and biosensing. *TRAC-Trends Anal Chem*. 2018;105:424–435. doi:10.1016/jtrac201805021
36. Ozcan N, Medetalibeyoglu H, Akyıldırım O, Atar N, Yola ML. Electrochemical detection of amyloid-β protein by delaminated titanium carbide MXene/multi-walled carbon nanotubes composite with molecularly imprinted polymer. *Mater Today Commun*. 2020;23:101097. doi:10.1016/jmtcomm2020101097
37. Cao H, Yu Q, Colby R, et al. Large-scale graphitic thin films synthesized on Ni and transferred to insulators: structural and electronic properties. *J Appl Phys*. 2010;107:44310. doi:10.1063/13309018
38. Song L, Ci L, Lu H, et al. Large scale growth and characterization of atomic hexagonal boron nitride layers. *Nano Lett*. 2010;10:3209. doi:10.1021/nl1022139
39. Lee YH, Zhang XQ, Zhang W, et al. Synthesis of large-area MoS2 atomic layers with chemical vapor deposition. *Adv Mater*. 2012;24:2320. doi:10.1002/adma201104798
40. Kara A, Enriquez H, Seitsonen AP, et al. A review on silicene – new candidate for electronics. *Surf Sci Rep*. 2012;67:1–18. doi:10.1016/jsurfrep201110001
41. Novoselov KS, Geim AK, Morozov SV, et al. Electric field effect in atomically thin carbon films. *Science*. 2004;306:666. doi:10.1126/science1102896

42. Kalantar-zadeh K, Vijayaraghavan A, Ham MH, Zheng H, Breedon M, Strano MS. Synthesis of atomically thin WO3 sheets from hydrated tungsten trioxide. *Chem Mater*. 2010;22:5660. doi:10.1021/cm1019603
43. McAllister MJ, Li JL, Adamson DH, et al. Single sheet functionalized graphene by oxidation and thermal expansion of graphite. *Chem Mater*. 2007;19:4396. doi:10.1021/cm0630800
44. Wang G, Yang J, Park J, et al. Facile synthesis and characterization of graphene nanosheets. *J Phys Chem C*. 2008;112:8192–8195. doi:10.1021/jp710931h
45. Mashtalir O, Naguib M, Dyatkin B, Gogotsi Y, Barsoum MW. Kinetics of aluminum extraction from Ti3AlC2 in hydrofluoric acid. *Mater Chem Phys*. 2013;139:147–152. doi:10.1016/jmatchemphys201301008
46. Wang X, Shen X, Gao Y, Wang Z, Yu R, Chen L. Atomic-scale recognition of surface structure and intercalation mechanism of Ti_3C_2X. *J Am Chem Soc*. 2015;137:2715–2721. doi:10.1021/ja512820k
47. Ghidiu M, Lukatskaya MR, Zhao MQ, Gogotsi Y, Barsoum MW. Conductive two-dimensional titanium carbide 'clay' with high volumetric capacitance. *Nature*. 2014;516:78–81. doi:10.1038/nature13970
48. Lind H, Wickman B, Halim J, Montserrat-Sisó G, Hellman A, Rosen J. Hydrogen evolution reaction for vacancy-ordered i-MXenes and the impact of proton absorption into the vacancies. *Adv Sustain Syst*. 2021;5:2000158. doi:10.1002/adsu202000158
49. Adibah NA, Zaine SA, Shukur MFA. Synthesis of Ti_3C_2 mxene through *in situ* hf and direct hf etching procedures as electrolyte fillers in dye-sensitized solar cell. *Mater Sci Forum*. 2021;1023:15–20. doi:10.4028/wwwscientificnet/MSF102315
50. Yang S, Zhang P, Wang F, et al. Fluoride-free synthesis of two-dimensional titanium carbide (MXene) using a binary aqueous system. *Angew Chem Int Ed*. 2018;57:15491–15495. doi:10.1002/anie201809662
51. Li T, Yao L, Liu Q, et al. Fluorine-free synthesis of high-purity $Ti_3C_2T_x$ (T=OH, O) via alkali treatment. *Angew Chem Int Ed*. 2018;57:6115–6119. doi:10.1002/anie201800887
52. Li Y, Shao H, Lin Z, et al. A general Lewis acidic etching route for preparing MXenes with enhanced electrochemical performance in non-aqueous electrolyte. *Nat Mater*. 2020;19:894–899. doi:10.1038/s41563-020-0657-0
53. Wu J, Wang Y, Zhang Y, et al. Highly safe and ionothermal synthesis of Ti_3C_2 MXene with expanded interlayer spacing for enhanced lithium storage. *J Energy Chem*. 2020;47:203–209. doi:10.1016/jjechem201911029
54. Pang SY, Wong Y-T, Yuan S, et al. Universal strategy for HF-free facile and rapid synthesis of two-dimensional MXenes as multifunctional energy materials. *J Am Chem Soc*. 2019;141:9610–9616. doi:10.1021/jacs9b02578
55. Huang P, Han WQ. Recent advances and perspectives of lewis acidic etching route: an emerging preparation strategy for mxenes. *Nano-Micro Lett*. 2023;15:68.
56. Li M, Lu J, Luo K, et al. Element replacement approach by reaction with Lewis acidic molten salts to synthesize nanolaminated MAX phases and MXene. *J Am Chem Soc*. 2019;141:4730–4737. doi:10.1021/jacs9b00574
57. Kamysbayev V, Filatov AS, Hu H, et al. Covalent surface modifications and superconductivity of two-dimensional metal carbide MXenes. *Science*. 2020;369:979–983. doi:10.1126/scienceaba8311
58. Sajid IH, Iqbal MZ, Rizwan S. Recent advances in the role of MXene-based hybrid architectures as electrocatalysts for water splitting. *RSC Adv*. 2024;14:6823–6847. doi:10.1039/D3RA06725D
59. Wang D, Filatov AS, Cho W, et al. Direct synthesis and chemical vapor deposition of 2D carbide and nitride MXenes. *Science*. 2023;379:1242–1247. doi:10.1126/scienceadd9204
60. Cai Y, Shen J, Ge G, et al. Stretchable $Ti_3C_2T_x$ MXene/carbon nanotube composite based strain sensor with ultrahigh sensitivity and tunable sensing range. *ACS Nano*. 2017;12:56–62. doi:10.1021/acsnano7b06251
61. Tian Y, Ju M, Luo Y, Bin X, Lou X, Que W. In situ oxygen doped $Ti_3C_2T_x$ MXene flexible film as supercapacitor electrode. *Chem Eng J*. 2022;446:137451. doi:10.1016/jcej2022137451
62. Kawai K, Fujita M, Iizuka R, Yamada A, Okubo M. Influence of surface termination groups on electrochemical charge storage of MXene electrodes. *2D Mater*. 2023;10:014012. doi:10.1088/2053-1583/aca1cf
63. Ma R, Chen Z, Zhao D, et al. $Ti_3C_2T_x$ MXene for electrode materials of supercapacitors. *J Mater Chem A*. 2021;9:11501–11529. doi:10.1039/D1TA00681A
64. Zeraati AS, Mirkhani SA, Sun P, Naguib M, Braun PV, Sundararaj U. Improved synthesis of $Ti_3C_2T_x$ MXenes resulting in exceptional electrical conductivity, high synthesis yield, and enhanced capacitance. *Nanoscale*. 2021;13:3572–3580. doi:10.1039/D0NR06671K
65. Aravind AM, Tomy M, Kuttapan A, Aippunny AMK, Suryabai XT. Progress of 2D MXene as an electrode architecture for advanced supercapacitors: a comprehensive review. *ACS Omega*. 2023;8:44375–44394. doi:10.1021/acsomega3c02002
66. Zhang YZ, El-Demellawi JK, Jiang Q, et al. MXene hydrogels: fundamentals and applications. *Chem Soc Rev*. 2020;49:7229–7251. doi:10.1039/D0CS00022A
67. Song F, Li G, Zhu Y, Wu Z, Xie X, Zhang N. Rising from the horizon: three-dimensional functional architectures assembled with MXene nanosheets. *J Mater Chem A*. 2020;8:18538–18559. doi:10.1039/D0TA06222G
68. Tang B, Yang Y, Shi Y, Nie H, Xia H, Shen X. Improved mechanical performances of short aramid fiber-reinforced polypropylene composites by Ti_3C_2 MXene nanosheets. *Polym Compos*. 2021;42:2010–2018. doi:10.1002/pc25953
69. Guo Z, Zhou J, Si C, Sun Z. Flexible two-dimensional $Ti_{n+1}C_n$ (n = 1, 2 and 3) and their functionalized MXenes predicted by density functional theories. *Phys Chem Chem Phys*. 2015;17:15348–15354. doi:10.1039/C5CP00775E
70. Kumar YA, Ramachandran T, Ghosh A, Al-Sehemi AG, Reddy NP. Md Moniruzzaman. *J Energy Storage*. 2025;121:116507. doi:10.1016/jest2025116507
71. Zhang HC, Guo YM. Advances of carbon quantum dots for fluorescence turn-on detection of reductive small biomolecules. *Chin J Anal Chem*. 2021;49:14–23. doi:10.1016/S1872-2040(20)60070-6
72. Xu X, Zhang H, Diao Q, Zhu Y, Yang G, Ma B. Highly sensitive fluorescent sensing for intracellular glutathione based on Ti_3C_2 quantum dots. *J Mater Sci Mater Electron*. 2020;31:175–181. doi:10.1007/s10854-019-02682-2
73. Liu M, He Y, Zhou J, Ge Y, Zhou J, Song G. A "naked-eye" colorimetric and ratiometric fluorescence probe for uric acid based on Ti_3C_2 MXene quantum dots. *Anal Chim Acta*. 2020;1103:134–142. doi:10.1016/jaca201912069
74. Zhu X, Pang X, Zhang Y, Yao S. Titanium carbide MXenes combined with red-emitting carbon dots as a unique turn-on fluorescent nanosensor for label-free determination of glucose. *J Mater Chem B*. 2019;7:7729–7735. doi:10.1039/C9TB02060H

75. Xia T, Liu G, Wang J, Hou S, Hou S. MXene-based enzymatic sensor for highly sensitive and selective detection of cholesterol. *Biosens Bioelectron*. 2021;183:113243. doi:10.1016/jbios2021113243
76. Shahzad F, Iqbal A, Zaidi SA, Hwang SW, Koo CM. Nafion-stabilized two-dimensional transition metal carbide ($Ti_3C_2T_x$ MXene) as a high-performance electrochemical sensor for neurotransmitter. *J Ind Eng Chem*. 2019;79:338–344. doi:10.1016/jjiec201903061
77. Zheng J, Wang B, Ding A, Weng B, Chen J. Synthesis of MXene/DNA/Pd/Pt nanocomposite for sensitive detection of dopamine. *J Electroanal Chem*. 2018;816:189–194. doi:10.1016/jjelechem201803056
78. Rakhi RB, Nayuk P, Xia C, Alshareef HN. Novel amperometric glucose biosensor based on MXene nanocomposite. *Sci Rep*. 2016;6:1–9. doi:10.1038/s41598-016-0001-8
79. Bharti A, Singh S, Munthala D, et al. Development of a nucleic acid-based screen-printed electrochemical biosensor using $Ti_3C_2T_x$ MXene for detection of SARS-CoV-2. *Microchem J*. 2023;195:109521. doi:10.1016/jmicroc2023109521
80. Chen WY, Lin H, Barui AK, Gomez AMU, Wendt MK, Stanciu LA. DNA-functionalized $Ti_3C_2T_x$ MXenes for selective and rapid detection of SARS-CoV-2 nucleocapsid gene. *ACS Appl Nano Mater*. 2022;5:1902–1910. doi:10.1021/acsanm1c03520
81. Wei W, Lin H, Hao T, et al. Dual-mode ECL/SERS immunoassay for ultrasensitive determination of Vibrio vulnificus based on multifunctional MXene. *Sens Actuators B Chem*. 2021;332:129525. doi:10.1016/jsnb2021129525
82. Subramania AK, Sugumaran S, Sethuramalingam P, Ramesh R, Dhandapani P, Angaiah S. $NiCo_2O_4/Ti_2NbC_2$ (double MXene) nanohybrid-based non-enzymatic electrochemical biosensor for detection of glucose in sweat. *Bioprocess Biosyst Eng*. 2023;46:1755–1763. doi:10.1007/s00449-023-02930-0
83. Peng X, Zhang Y, Lu D, Guo Y, Guo S. Ultrathin Ti_3C_2 nanosheets-based "off-on" fluorescent nanoprobe for rapid and sensitive detection of HPV infection. *Sens Actuators B Chem*. 2019;286:222–229. doi:10.1016/jsnb201901158
84. Hantanasirisakul K, Gogotsi Y. Electronic and optical properties of 2D transition metal carbides and nitrides (MXenes). *Adv Mater*. 2018;30:1804779. doi:10.1002/adma201804779
85. Zhang J, Li Y, Duan S, He F. Highly electrically conductive two-dimensional Ti_3C_2 MXenes-based 16S rDNA electrochemical sensor for detecting Mycobacterium tuberculosis. *Anal Chim Acta*. 2020;1123:9–17. doi:10.1016/jaca202005013
86. Patra I, Kammoud MK, Al-qaim HA, et al. Perspectives and trends in advanced MXenes-based optical biosensors for the recognition of food contaminants. *Crit Rev Anal Chem*. 2024;54:633–652. doi:10.1080/1040834720222091921
87. Hsu CY, Alshik NMM, Ahmad I, et al. Recent advances in MXene nanozyme-based optical and electrochemical biosensors for food safety analysis. *Nanoscale*. 2025;17:7697–7712. doi:10.1039/D5NR00066A
88. Al-Hawary SI, Sapaev IB, Althomali RH, et al. Recent progress in screening of mycotoxins using MXenes-based nanomaterials. *Crit Rev Anal Chem*. 2024;54:3066–3082. doi:10.1080/1040834720232222412
89. Magesh V, Nagarajan RD, Sridharan G, et al. Sensor technologies for food quality and safety. *R Soc Chem*. 2025;29:175–228.
90. Syraji Y, Jeyaramraja PR, Mada T, Gobikanila K. Comprehensive review of aflatoxin contamination, effects, management, and perspectives. *Discov Food*. 2025;5:377. doi:10.1007/s44187-025-00680-4
91. Wu Z, Sun DW, Pu H, Wei Q, Lin X. Ti_3C_2Tx MXenes loaded with Au nanoparticle dimers as a surface-enhanced Raman scattering aptasensor for AFB1 detection. *Food Chem*. 2022;372:131293. doi:10.1016/jfoodchem2021131293
92. Xu G, Niu Y, Yang X, et al. Preparation of $Ti_3C_2T_x$ MXene-derived quantum dots with white/blue emission and electrochemiluminescence. *Adv Opt Mater*. 2018;6:1800951. doi:10.1002/adom201800951
93. Wang H, Li H, Huang Y, Xiong M, Wang F, Li C. A label-free electrochemical biosensor for highly sensitive detection of gliotoxin based on DNA nanostructure/MXene nanocomplexes. *Biosens Bioelectron*. 2019;142:111531. doi:10.1016/jbios2019111531
94. Tang J, Liu X, Yang C, et al. A carbon-rich nanofiber framework based on a conjugated arylacetylene polymer for photocathodic enzymatic bioanalysis. *RSC Adv*. 2019;9:42533–42542. doi:10.1039/C9RA09157B
95. Liu H, Duan C, Yang C, Shen W, Wang F, Zhu Z. A novel nitrite biosensor based on the direct electrochemistry of hemoglobin immobilized on MXene- Ti_3C_2. *Sens Actuators B Chem*. 2015;218:60–66. doi:10.1016/jsnb201504090
96. Song D, Jiang X, Li Y, et al. Metal–organic frameworks-derived MnO_2/Mn_3O_4 microcuboids with hierarchically ordered nanosheets and Ti_3C_2 MXene/Au NPs composites for electrochemical pesticide detection. *J Hazard Mater*. 2019;373:367–376. doi:10.1016/jjhazmat201903083
97. Guan Q, Ma J, Yang W, et al. Highly fluorescent Ti_3C_2 MXene quantum dots for macrophage labeling and Cu^{2+} ion sensing. *Nanoscale*. 2019;11:14123–14133. doi:10.1039/C9NR04421C
98. Yang G, Zhao J, Yi S, Wan X, Tang J. Biodegradable and photostable Nb_2C MXene quantum dots as promising nanofluorophores for metal ions sensing and fluorescence imaging. *Sens Actuators B Chem*. 2020;309:127735. doi:10.1016/jsnb2020127735
99. Rathi K, Arkoti NK, Pal K. Fabrication of Delaminated 2D Metal Carbide MXenes (Nb_2CT) by CTAB-based NO_2 gas sensor with enhanced stability. *Adv Mater Interfaces*. 2022;9:2200415. doi:10.1002/admi202200415
100. Gao G, OMullane AP, Du A. 2D MXenes: a new family of promising catalysts for the hydrogen evolution reaction. *ACS Catal*. 2017;7:494–500. doi:10.1021/acscatal6b02754
101. Jiang Y, Sun T, Xie X, et al. Oxygen-functionalized ultrathin $Ti_3C_2T_x$ MXene for enhanced electrocatalytic hydrogen evolution. *Chem SusChem*. 2019;12:1368–1373. doi:10.1002/cssc201803032
102. Xie Y, Naguib M, Mochalin VN, et al. Role of surface structure on Li-ion energy storage capacity of two-dimensional transition-metal carbides. *J Am Chem Soc*. 2014;136:6385–6394. doi:10.1021/ja501520b
103. Wang Y, Mao J, Meng X, Yu L, Deng D, Bao X. Catalysis with two-dimensional materials confining single atoms: concept, design, and applications. *Chem Rev*. 2019;119:1806–1854. doi:10.1021/acschemrev8b00501
104. Huang B, Zhou N, Chen X, Ong WJ, Li N. Insights into the electrocatalytic hydrogen evolution reaction mechanism on two-dimensional transition metal carbonitrides (MXene). *Chem Eur J*. 2018;24:18479–18486. doi:10.1002/chem201804686
105. Li P, Zhu J, Handoko AD, et al. High-throughput theoretical optimization of the hydrogen evolution reaction on MXenes by transition metal modification. *J Mater Chem A*. 2018;6:4271–4278. doi:10.1039/C8TA00173A
106. Zhao D, Chen Z, Yang W, et al. MXene (Ti_3C_2) vacancy-confined single-atom catalyst for efficient functionalization of CO_2. *J Am Chem Soc*. 2019;141:4086–4093. doi:10.1021/jacs8b13579
107. Kuznetsov DA, Chen Z, Kumar PV, et al. Single site cobalt substitution in 2D molybdenum carbide (MXene) enhances catalytic activity in the hydrogen evolution reaction. *J Am Chem Soc*. 2019;141:17809–17816. doi:10.1021/jacs9b08897

108. Zhang J, Zhao Y, Guo X, et al. Single platinum atoms immobilized on an MXene as an efficient catalyst for the hydrogen evolution reaction. *Nat Catal*. 2018;1:985–992. doi:10.1038/s41929-018-0195-1
109. Zhang T, Jiang X, Li G, Yao Q, Lee J. A red-phosphorous-assisted ball-milling synthesis of few-layered $Ti_3C_2T_x$ (MXene) nanodot composite. *ChemNanoMat*. 2018;4:56–60. doi:10.1002/cnma201700232
110. Saidur R, Mushtaq A, Huang S, et al. Synthesis of ultra-small MXene nanorods for enhanced photothermal therapy of breast cancer in vitro. *Mater Lett*. 2023;353:135324. doi:10.1016/jmatlet2023135324
111. Yuan W, Cheng L, An Y, et al. MXene nanofibers as highly active catalysts for hydrogen evolution reaction. *ACS Sustain Chem Eng*. 2018;6:8976–8982. doi:10.1021/acssuschemeng8b01348
112. Huang L, Ai L, Wang M, Jiang J, Wang S. Hierarchical MoS_2 nanosheets integrated Ti_3C_2 MXenes for electrocatalytic hydrogen evolution. *Int J Hydrogen Energy*. 2019;44:965–976. doi:10.1016/jijhydene201811084
113. Yu M, Wang Z, Liu J, Sun F, Yang P, Qiu J. A hierarchically porous and hydrophilic 3D nickel–iron/MXene electrode for accelerating oxygen and hydrogen evolution at high current densities. *Nano Energy*. 2019;63:103880. doi:10.1016/jnanoen2019103880
114. Xiu L, Wang Z, Yu M, Wu X, Qiu J. Aggregation-resistant 3D MXene-based architecture as efficient bifunctional electrocatalyst for overall water splitting. *ACS Nano*. 2018;12:8017–8028. doi:10.1021/acsnano8b02849
115. Filip J, Zavahir S, Lorencova L, et al. Tailoring electrocatalytic properties of Pt nanoparticles grown on $Ti_3C_2T_x$ MXene surface. *J Electrochem Soc*. 2019;166:H54–H62. doi:10.1149/20991902jes
116. Zhu X, Xie Y, Liu Y. Exploring the synergy of 2D MXene-supported black phosphorus quantum dots in hydrogen and oxygen evolution reactions. *J Mater Chem A*. 2018;6:21255–21260. doi:10.1039/C8TA08374F
117. Liu J, Liu Y, Xu D, et al. Hierarchical "nanoroll"-like $MoS_2/Ti_3C_2T_x$ hybrid with high electrocatalytic hydrogen evolution activity. *Appl Catal B*. 2019;241:89–94. doi:10.1016/japcatb201808083
118. Lian P, Dong Y, Wu Z-S, et al. Alkalized Ti_3C_2 MXene nanoribbons with expanded interlayer spacing for high-capacity sodium and potassium ion batteries. *Nano Energy*. 2017;40:1–8. doi:10.1016/jnanoen201708002
119. Kuang P, He M, Zhu B, Yu J, Fan K, Jaroniec M. 0D/2D NiS_2/V-MXene composite for electrocatalytic H2 evolution. *J Catal*. 2019;375:8–20. doi:10.1016/jjcat201905019
120. Wang Z, Xu W, Yu K, Feng Y, Zhu Z. 2D-heterogeneous vanadium compound interfacial modulation enhanced synergistic catalytic hydrogen evolution for full pH range seawater splitting. *Nanoscale*. 2020;12:6176–6187. doi:10.1039/D0NR00207K
121. Huang J, Liu X-Q, Meng -F-F, et al. A facile method to produce $MoSe_2$/MXene hybrid nanoflowers with enhanced electrocatalytic activity for hydrogen evolution. *J Electroanal Chem*. 2020;856:113727. doi:10.1016/jjelechem2019113727
122. Li Z, Qi Z, Wang S, et al. In situ formed Pt_3Ti nanoparticles on a two-dimensional transition metal carbide (MXene) used as efficient catalysts for hydrogen evolution reactions. *Nano Lett*. 2019;19:5102–5108. doi:10.1021/acsnanolett9b01381
123. Wang J, He P, Shen Y, et al. FeNi nanoparticles on Mo_2TiC_2Tx MXene@nickel foam as robust electrocatalysts for overall water splitting. *Nano Res*. 2021;14:3474–3481. doi:10.1007/s12274-021-3660-0
124. Huang TY, Yang Z, Yang SY, et al. Construction of 2D/2D $Ti_3C_2T_x$ MXene/CdS heterojunction with photothermal effect for efficient photocatalytic hydrogen production. *J Mater Sci Technol*. 2024;171:1–9. doi:10.1016/jjmst202307010
125. Ran J, Gao G, Li FT, Ma TY, Du A, Qiao SZ. Ti_3C_2 MXene co-catalyst on metal sulfide photo-absorbers for enhanced visible-light photocatalytic hydrogen production. *Nat Commun*. 2017;8:13907. doi:10.1038/ncomms13907
126. Huang J, Tao J, Liu G, Lu L, Tang H, Qiao G. In situ construction of 1D CdS/2D Nb_2CT_x MXene Schottky heterojunction for enhanced photocatalytic hydrogen production activity. *Appl Surf Sci*. 2022;573:151491. doi:10.1016/japsusc2021151491
127. Sherryna A, Tahir M, Zakaria ZY. Well-structured V2C MXenes coupled g-C_3N_4 2D/2D nanohybrids for proficient charge separation with the role of triethanolamine (TEOA) as a protective barrier of g-C_3N_4 for stimulating photocatalytic H2 production. *Int J Hydrogen Energy*. 2024;51:1511–1531. doi:10.1016/jijhydene202309234
128. Li Y, Ding L, Guo Y, Liang Z, Cui H, Tian J. Boosting the photocatalytic ability of g-C3N4 for hydrogen production by Ti_3C_2 MXene quantum dots. *ACS Appl Mater Interfaces*. 2019;11:41440–41447. doi:10.1021/acsami9b14985
129. Kang J, Byun S, Kim S, et al. Design of three-dimensional hollow-sphere architecture of $Ti_3C_2T_x$ MXene with graphitic carbon nitride nanoshells for efficient photocatalytic hydrogen evolution. *ACS Appl Energy Mater*. 2020;3:9226–9233. doi:10.1021/acsaem0c01590
130. Liu D, Li C, Ge J, et al. 3D interconnected g-C_3N_4 hybridized with 2D Ti3C2 MXene nanosheets for enhancing visible light photocatalytic hydrogen evolution and dye contaminant elimination. *Appl Surf Sci*. 2022;579:152180. doi:10.1016/japsusc2021152180
131. Li Y, Yin Z, Ji G, et al. 2D/2D/2D heterojunction of Ti_3C_2 MXene/MoS_2 nanosheets/TiO_2 nanosheets with exposed (001) facets toward enhanced photocatalytic hydrogen production activity. *Appl Catal B*. 2019;246:12–20. doi:10.1016/japcatb201901051
132. Yang JX, Yu WB, Li CF, et al. PtO nanodots promoting Ti_3C_2 MXene in-situ converted Ti_3C_2/TiO_2 composites for photocatalytic hydrogen production. *Chem Eng J*. 2021;420:129695. doi:10.1016/jcej2021129695
133. Sun Y, Hao Y, Lin X, et al. Efficient electron transport by 1D CuZnInS modified 2D Ti_3C_2 MXene for enhanced photocatalytic hydrogen production. *J Colloid Interface Sci*. 2024;653:396–404. doi:10.1016/jjcis202309075
134. Zhang J, Xing C, Shi F. MoS_2/Ti_3C_2 heterostructure for efficient visible-light photocatalytic hydrogen generation. *Int J Hydrogen Energy*. 2020;45:6291–6301. doi:10.1016/jijhydene201912109
135. Yao Q, Wang L, Tian Y, Li P. One-step synthesis of multiple electron migration channels $TiO_2/Fe_2O_3@Ti_3C_2$ MXene heterojunction composite for high-efficiency photocatalytic hydrogen production. *Opt Mater*. 2023;142:114018. doi:10.1016/joptmat2023114018
136. Varadarajan S, Kavitha A, Selvaraju P, et al. Enhanced photocatalytic hydrogen evolution by TiO_2: a synergistic approach with defect-rich SnS_2 and Ti_3C_2 MXene cocatalysts. *Hydrogen*. 2024;5:940–957. doi:10.3390/hydrogen5040050
137. Bai J, Shen R, Jiang Z, Zhang P, Li Y, Li X. Integration of 2D layered CdS/WO_3 S-scheme heterojunctions and metallic Ti_3C_2 MXene-based ohmic junctions for effective photocatalytic H2 generation. *Chin J Catal*. 2022;43:359–369. doi:10.1016/S1872-2067(21)63883-4
138. Hieu VQ, Lam TC, Khan A, et al. TiO_2/Ti_3C_2/g-C_3N_4 ternary heterojunction for photocatalytic hydrogen evolution. *Chemosphere*. 2021;285:131429. doi:10.1016/jchemosphere2021131429
139. Chen X, Guo Y, Bian R, et al. Titanium carbide MXenes coupled with cadmium sulfide nanosheets as two-dimensional/two-dimensional heterostructures for photocatalytic hydrogen production. *J Colloid Interface Sci*. 2022;613:644–651. doi:10.1016/jjcis202201079

140. Wang Y, Wang X, Ji Y, et al. Ti_3C_2 MXene coupled with CdS nanoflowers as 2D/3D heterostructures for enhanced photocatalytic hydrogen production activity. *Int J Hydrogen Energy*. 2022;47:22045–22053. doi:10.1016/jijhydene202205014
141. Xiao Y, Zhang W. High throughput screening of M_3C_2 MXenes for efficient CO2 reduction conversion into hydrocarbon fuels. *Nanoscale*. 2020;12:7660–7673. doi:10.1039/C9NR10598K
142. Ding M, Xiao R, Zhao C, et al. Evidencing interfacial charge transfer in 2D CdS/2D MXene Schottky heterojunctions toward high-efficiency photocatalytic hydrogen production. *Sol RRL*. 2021;5:2000414. doi:10.1002/solr202000414
143. Wong KJ, Foo JJ, Siang TJ, Khoo V, Ong W. Harnessing the power of light: the synergistic effects of crystalline carbon nitride and $Ti_3C_2T_x$ MXene in photocatalytic hydrogen production. *Glob Chall*. 2024;8:2300235. doi:10.1002/gch2202300235
144. Shao M, Shao Y, Ding S, et al. Carbonized MoS_2: super-active co-catalyst for highly efficient water splitting on CdS. *ACS Sustain Chem Eng*. 2019;7:4220–4229. doi:10.1021/acssuschemeng8b05917
145. Kibsgaard J, Tsai C, Chan K, et al. Designing an improved transition metal phosphide catalyst for hydrogen evolution using experimental and theoretical trends. *Energy Environ Sci*. 2015;8:3022–3029. doi:10.1039/C5EE02179K
146. Bai S, Yang M, Jiang J, et al. Recent advances of MXenes as electrocatalysts for hydrogen evolution reaction. *NPJ 2D Mater Appl*. 2021;5:78. doi:10.1038/s41699-021-00259-4
147. Marquez KP, Sisican KMD, Ibabao RP, et al. Understanding the chemical degradation of $Ti_3C_2T_x$ MXene dispersions: a chronological analysis. *Small Sci*. 2024;4:2400150. doi:10.1002/smsc202400150
148. Mashtalir O, Cook KM, Mochalin VN, Crowe M, Barsoum MW, Gogotsi Y. Dye adsorption and decomposition on two-dimensional titanium carbide in aqueous media. *J Mater Chem A*. 2014;2:14334. doi:10.1039/C4TA02638A
149. Lipatov A, Alhabeb M, Lukatskaya MR, Boson A, Gogotsi Y, Sinitskii A. Effect of synthesis on quality, electronic properties and environmental stability of individual monolayer ti_3c_2 mxene flakes. *Adv Electron Mater*. 2016;2:1600255. doi:10.1002/aelm201600255
150. Maleski K, Mochalin VN, Gogotsi Y. Dispersions of two-dimensional titanium carbide mxene in organic solvents. *Chem Mater*. 2017;29:1632. doi:10.1021/acschemmater6b04830
151. Wu T, Kent PRC, Gogotsi Y, D-e J. How Water Attacks MXene. *Chem Mater*. 2022;34:4975. doi:10.1021/acschemmater2c00224
152. Zhao X, Cao H, Coleman BJ, et al. The role of antioxidant structure in mitigating oxidation in $Ti_3C_2T_x$ and Ti_2CT_x MXenes. *Adv Mater Interfaces*. 2022;9:2200480. doi:10.1002/admi202200480